Redox and osmotic homeostasis: Central drivers of drought resilience in grapevine rootstocks

Ahmed Ismail [a,b,c], Pranavkumar Gajjar [a], Ahmed G. Darwish [d], Eman Abuslima [e],
Tabibul Islam [f], Ahmed G. Mohamed [a], Violeta Tsolova [a], Peter Nick [g], Walid El Kayal [h,**],
Islam El-Sharkawy [a,*]

[a] Center for Viticulture and Small Fruit Research, College of Agriculture and Food Sciences, Florida A&M University, Tallahassee, FL, 32308, USA
[b] Department of Botany and Plant Sciences, University of California Riverside, Riverside, CA, 92521, USA
[c] Department of Horticulture, Faculty of Agriculture, Damanhour University, Damanhour, 22516, Egypt
[d] Department of Horticultural Sciences, Texas A&M University, College Station, TX, 77843, USA
[e] Department of Botany and Microbiology, Faculty of Science, Suez Canal University, Ismailia, 41522, Egypt
[f] Plant Sciences Department, University of Tennessee, Knoxville, TN, 37996, USA
[g] Molecular Cell Biology, Joseph Gottlieb Kölreuter Institute for Plant Sciences, Karlsruhe Institute of Technology (KIT), 76131, Germany
[h] Faculty of Agricultural and Food Sciences, American University of Beirut, Beirut, 1107-2020, Lebanon

ARTICLE INFO

ABSTRACT

A comparative study of two grapevine rootstocks with contrasting drought stress responses revealed that the drought-resilient RUG harbors an efficient antioxidant defense system, characterized by increased activities of superoxide dismutase (SOD), glutathione peroxidase (GPX), and catalase (CAT), along with elevated proline (Pro) levels compared to the drought-sensitive MGT. This robust scavenging machinery enables RUG to maintain redox balance, effectively mitigating oxidative stress and preserving cellular integrity during drought. Anatomical evaluations showed severe xylem disruptions in MGT, including extensive tylosis, leading to leaf necrosis and impaired water transport. Conversely, RUG maintained a structurally intact and functional xylem, crucial for sustaining hydraulic conductivity and water supply during drought. The pronounced rise in Pro underscores its critical role in drought resilience, working synergistically with other cellular components to facilitate osmotic adjustment while detoxifying reactive oxygen species (ROS) and minimizing oxidative damage. Transcriptome profiling suggested that RUG displays sequential gene expression during drought driven by distinct molecular processes for photosynthesis, osmotic adjustment, and structural remodeling, a dynamic notably absent in MGT. These findings emphasize the complex interplay of osmotic and oxidative homeostasis in RUG, illustrating the adaptive mechanisms that contribute to its drought resilience, potentially guiding future rootstock selection and breeding strategies.

1. Introduction

Plant biotic/abiotic stresses have severe impacts on agriculture, leading to annual crop yield losses estimated at 65–87% (Shinozaki et al., 2015). Climate change is likely to exacerbate these losses as extreme weather events become more frequent (www.fao.org). Drought occurs when rainfall decreases or stops, reducing soil water potential while increasing osmotic potential. This imbalance hinders water uptake through roots compared to transpiration from leaves, raising tension in the water column and potentially causing embolism in xylem vessels under severe dehydration (Gambetta et al., 2020). Drought stress disrupts essential biological processes in plants, particularly photosynthesis and energy production while triggering harmful cellular and molecular responses such as oxidative bursts, metabolic toxicity, and protein dysfunction (Ismail et al., 2014, 2020; Kim et al., 2024). Ultimately, these effects compromise plant growth, resilience, and productivity, highlighting the necessity for adaptive strategies to enhance drought tolerance.

* Corresponding author.
** Corresponding author.
E-mail addresses: we21@aub.edu.lb (W. El Kayal), islam.elsharkawy@famu.edu (I. El-Sharkawy).

In contrast to sensitive species, drought-tolerant plants activate rapid and robust resilience mechanisms upon stress exposure, effectively mitigating damage. A key aspect of this resilience is the reactive oxygen species (ROS) detoxification system, which enables plants to neutralize harmful ROS, such as hydrogen peroxide (H_2O_2), superoxide (O^{2-}), and hydroxyl radicals ($OH^\bullet$). These ROS are commonly produced under stress and are unavoidable by-products of essential aerobic metabolic processes like photosynthesis and respiration (Miller et al., 2010; Waszczak et al., 2018). The antioxidant defense system consists of enzymatic components, including superoxide dismutase (SOD), glutathione peroxidase (GPX), ascorbate peroxidase (APX), peroxidase (POX), glutathione reductase (GR), glutathione-S-transferase (GST), and catalase (CAT), which detoxify excessive ROS (Rajput et al., 2021). Additionally, non-enzymatic antioxidants such as phenolic compounds, alkaloids, carotenoids, ascorbic acid, glutathione (GSH), flavonoids, phenolic acids, tannins, terpenoids, alkaloids, and proline (Pro) help neutralize ROS effects (Das and Roychoudhury, 2014; Haghpanah et al., 2024).

Proline further functions as a vital compatible osmolyte, playing a critical role in regulating osmotic balance under conditions of water deficit. It works in conjunction with a diverse array of solutes, categorized into various classes according to their characteristics, including (1) osmolytes containing ammonium compounds (e.g., glycine betaine and polyamines), (2) osmolytes containing sugars and sugar alcohols (e.g., fructose, glucose, sucrose, trehalose, fructans, mannitol, sorbitol, and glycerol), (3) osmolytes containing amino acids (e.g., proline, citrulline, pipecolic acid, and ectoine), and osmolytes containing sulfonium compounds (e.g., choline *o*-sulfate and dimethyl sulfonium propionate) (Turner, 2018; Takahashi et al., 2020; Nour et al., 2024). Osmotic imbalance, a specific outcome of water stress, underscores the necessity for targeted mechanisms that bolster plant resilience to drought conditions. Consequently, osmotic adjustment emerges as a crucial strategy for preserving cell turgor, mitigating water loss, and sustaining metabolic activities during periods of stress. Interestingly, both proline and glycine-betaine can significantly alter the osmotic potential of the cytoplasm and vacuole, accounting for ~10% and 90% of cell volume, respectively. These compounds not only facilitate osmotic balance but also provide protective functions by stabilizing proteins and cellular membranes and scavenging ROS in stressed cells (Bohnert and Shen, 1998; Turner, 2018). Collectively, these adaptive responses empower tolerant plants to maintain cellular stability and functionality, even in challenging environmental conditions.

Grapevine, a valuable cash crop cultivated in over 90 countries, faces increasing threats from water-related stresses, particularly due to climate change, affecting grape quality and yield (Gambetta et al., 2020). Thus, understanding the mechanisms underlying grapevine resilience to drought and other stresses is critical for breeding new, stress-resistant genotypes and rootstocks. Our previous studies highlighted the physiological responses of two salt-excluder grape rootstocks, RUG and MGT, under salinity stress, revealing RUG's superior ability to maintain photosynthetic pigments, sugars, and ROS detoxification compared to MGT (Gajjar et al., 2023, 2024). Although salinity and drought stress vary, some mechanistic overlaps exist, with RUG primarily recognized for drought tolerance. This study aims to profile the physiological, anatomical, and transcriptomic responses of RUG and MGT under drought and rewatering. Our findings provide insights into the molecular events that enhance grapevine drought resilience, revealing that RUG rapidly adjusts via transcriptomic reprogramming to promote redox and osmotic homeostasis. This redox mechanism maintains ROS balance by managing photorespiration-derived ROS, preventing cellular damage, while osmotic regulation protects xylem vessels from embolism and cavitation through transpiration moderation via stomatal control. Together, these mechanisms enhance RUG's drought resilience, supporting its potential as a valuable rootstock in drought-prone areas.

2. Materials and methods

2.1. Plant material of drought-stressed grapevine

The experiment was conducted in a greenhouse at the Center for Viticulture in Tallahassee, Florida (30°28′45.63″ N, 84°10′16.43″ W). Three-year-old *Vitis* hybrid rootstocks, Millardet et de Grasset 420A (MGT; *V. berlandieri* × *V. riparia*) and 140 Ruggeri (RUG; *V. berlandieri* × *V. rupestris*) were selected in this study due to their contrasting drought resilience characteristics. Grapevine seedlings were grown in 2.0 L plastic pots, which were filled with a growing medium composed of sandy soil, vermiculite, and humus in a 1:1:1 vol ratio. The greenhouse maintained a consistent air temperature of 25 °C during the day and 18 °C at night, regulated by a thermostat. Conditions of relative humidity and light levels were not specifically controlled, and no supplementary lighting was provided. All vine seedlings were grown under the same conditions; however, control vines were irrigated every two days. Other management practices adhered to the recommendations detailed in the Grape Production Guide for Florida, developed by the Center for Viticulture and Small Fruit Research (CVSFR) at Florida Agricultural and Mechanical University (FAMU) (https://famu.edu/viticulture). For morphological analysis, stomatal size and density were examined using a Leica stereo microscope, with images captured by a Leica DFC3000G digital camera and analyzed using the LAS X integrated imaging system (Leica, Deerfield, IL, USA). Leaf length, width, and area were measured following standard protocols. Transpiration rates were recorded over seven days to assess water loss behavior under controlled conditions.

In the PEG-induced drought stress assay, leaf samples from RUG and MGT were placed in Petri dishes containing double layers of wet paper towels saturated with PEG-6000 (10% w/v) and incubated for 24 h. Following treatment, samples (n = 3 biological replicates) were collected to quantify membrane integrity by ion leakage analysis. The PEG-treated samples were rinsed to remove surface ions, placed in distilled water, and agitated at 25 °C for 24 h. Initial conductivity, indicating membrane leakage, was measured using the YSI 3200 Conductivity Instrument (VWR, Suwanee, GA, USA). Samples were then boiled to release all cellular ions for total conductivity measurement, and relative ion leakage was calculated as the ratio of initial to total conductivity. A time-course experiment was conducted, with samples (n = 3 biological replicates) collected at 0, 6, 12, 24, and 48 h post PEG treatment. Cell viability was assessed using the MTT Tetrazolium Reduction Assay (Ginouves et al., 2014). Briefly, samples were treated with MTT solution (0.5 mg/ml) and incubated in the dark for 4 h. Formazan, indicative of viable cells, was quantified by measuring absorbance at 570 nm using an ACCURIS Smart microplate reader.

For drought experiments on grapevine seedlings, stress was induced by gradually withholding water to allow soil water content (SWC) to decline naturally. The relative fluorescence decrease (Rfd) was measured during stress using the Fluorpen FP110-LM/D (Qubit Systems Inc., Kingston, ON, Canada). Leaf samples were collected at specific SWC levels (60%, 40%, and 35%) and 4 and 12 days post-rewatering, while control samples were taken from plants receiving standard irrigation. The sampling sequence was as follows: (1) control, (2) 60% SWC, (3) 40% SWC, (4) 35% SWC, (5) day 4 post-rewatering, and (6) day 12 post-rewatering. Other two sets of samples; 80% SWC and day 8 post-rewatering, were collected for detailed analysis. All samples were immediately frozen in liquid nitrogen and stored at −80 °C for further analysis.

2.2. Photosynthetic pigments quantification

Photosynthetic pigments (PhPs), including total chlorophyll (Chl-T), chlorophyll-a (Chl-a), chlorophyll-b (Chl-b), and carotenoids, were quantified using the dimethyl sulfoxide (DMSO) method as outlined by Minocha et al. (2009). Briefly, 50 mg of leaf tissue was homogenized in 1.5 ml of DMSO, incubated in a water bath at 65 °C for 1 h, then cooled

to room temperature for 30 min. The mixture was filtered, shaken, and absorbance was measured at 665, 648, and 480 nm for Chl-a, Chl-b, and β-carotene, respectively, using an ACCURIS Smart microplate reader, with DMSO as a blank. Pigment concentrations were determined in triplicate for each biological replicate ($n = 9$) and expressed as mg/g fresh weight. Concentrations of Chl-a, Chl-b, and β-carotene were calculated as described previously by Gajjar et al. (2023).

2.3. Quantification of H₂O₂ content

Hydrogen peroxide (H₂O₂) content was measured following the method of Islam et al. (2017). Briefly, 100 mg of fresh, powdered leaf tissue was mixed with 1 ml of 50 mM potassium phosphate buffer (pH 7.8). The mixture was then centrifuged at $12,000 \times g$ for 10 min at 4 °C. For H₂O₂ quantification, the supernatant was combined with 0.1% titanium chloride in 20% (v/v) H₂SO₄ and centrifuged at $10,000 \times g$ for 5 min. Absorbance was recorded at 410 nm using a microplate reader (ACCURIS SmartReader). H₂O₂ levels were calculated using an extinction coefficient of 0.28 $\mu mol^{-1}\ cm^{-1}$.

2.4. Quantification of enzymatic antioxidants

To quantify antioxidant enzyme activity, 100 mg of fresh, ground leaf tissue was homogenized in 50 mM potassium phosphate buffer (pH 7.0) and centrifuged at $12,000 \times g$ for 10 min. The supernatant was used for total protein measurement and enzyme activity assays. Total protein content was determined using the Bradford assay, with bovine serum albumin (BSA) as the standard (Bradford, 1976). The activities of superoxide dismutase (SOD), catalase (CAT), and glutathione peroxidase (GPX) were measured using BioVision Inc. assay kits (Milpitas, CA, USA), following the manufacturer's instructions, and expressed as U/mg protein. One unit of SOD is defined as the amount of enzyme needed to achieve a 50% reduction in formazan dye formation, while SOD inhibition activity was also expressed in U/mg protein. CAT activity is defined as the amount of enzyme that decomposes 1.0 nmol of H₂O₂ min^{-1}, and GPX activity is defined as the amount of enzyme that reduces 1.0 nmol of NADPH min^{-1}.

2.5. Proline quantification

A 100 mg of powder leaf tissue was extracted with 3% sulfosalicylic acid and then centrifuged. The supernatant was mixed with a ninhydrin solution containing acetic acid and 6 M H₃PO₄ (v/v, 3:2) and heated at 100 °C for 60 min. Then, toluene was added to the mixture and incubated at room temperature for 30 min. Absorbance was measured in the toluene layer at 520 nm using a microplate reader (ACCURIS SmartReader), with quantification based on an L-proline standard curve (1–100 μg), as previously described by Lee et al. (2013).

2.6. Soluble sugar quantification

Fresh leaf tissue (100 mg) was ground in 1 mL of 80% ethanol, vortexed, and then centrifuged at $12,000 \times g$ for 10 min, following the method outlined in Gajjar et al. (2023). The supernatant was collected, and the extraction was repeated twice. Glucose, sucrose, and fructose levels were quantified using the Megazyme Sucrose/D-Fructose/D-Glucose Assay Kit (Megazyme, Highland, UT, USA), following the manufacturer's instructions. Total soluble sugar content was calculated by summing the individual concentrations of glucose, fructose, and sucrose in each sample.

2.7. Scanning electron microscope (SEM) analysis

Sample preparation was performed as described previously by El Kayal et al. (2017). Stem tissues were fixed in a solution of 2.5% glutaraldehyde and 2% paraformaldehyde in 0.1 M phosphate buffer, then washed three times with 0.1 M phosphate buffer for 10 min each. After fixation, samples underwent an ethanol dehydration series, followed by three 30-min immersions in 100% hexamethyldisilazane (HMDS). Following the final immersion, samples were left in HMDS until complete evaporation. The samples were then sputter-coated with carbon using a Nanotek SEMprep 2 sputter coater. Imaging and quantitative analysis were conducted using a Tescan MIRA3 scanning electron microscope.

2.8. RNA extraction and RNA-seq library construction

Total RNA was extracted from leaf samples as described previously (Gajjar et al., 2024). All RNA samples were treated with the RNase-Free DNase Set (Qiagen, Valencia, CA, USA), and subsequently cleaned up with the RNeasy Mini Kit (Qiagen). A total of 36 RNA-seq libraries (6-time points × 2 rootstocks (RUG and MGT) × 3 biological replicates) were constructed using NEBNext Ultra II RNA Library Prep Kit for Illumina (New England Biolabs, Ipswich, MA, USA). The libraries were multiplexed equally for paired-end 150-base sequencing in two lanes of NovaSeq 6000 (Illumina, San Diego, CA, USA) at the Novogene Co., Ltd. (Sacramento, CA, USA).

2.9. Sequencing data preprocessing and analysis

Illumina sequencing of multiplexed RNA-seq libraries produced 36 FASTQ files (GenBank accession: PRJNA1045631). The RNA-seq analysis pipeline was described previously by Ismail et al. (2022). Briefly, the quality assessment of reads was conducted twice, before and after trimming with Trimmomatic v0.39 using FastQC (Bolger et al., 2014). Trimmed reads were then aligned to the *Vitis* genome (*V. vinifera*_457_Genoscope.12X) and mapped to the *Vitis* transcriptome (*V. vinifera*_457_v2.1.cds_primaryTranscriptOnly.fa.gz) via STAR (Dobin et al., 2013; Srivastava et al., 2020). The STAR-generated BAM files were quantified using Salmon's alignment mode (Patro et al., 2017; Table S1). Differential gene expression was analyzed for each timepoint within rootstocks, RUG (R2-R1 through R6-R5) and MGT (M2-M1 through M6-M5), and between RUG and MGT timepoints, using DESeq2 with $P_{FDR} < 0.05$ (Love et al., 2014; Table S2). UpSetR was used to visualize intersections of differentially expressed genes across comparisons (Conway et al., 2017), while consensus Venn diagrams were created using "Draw Venn diagram" (https://bioinformatics.psb.ugent.be/webtools/Venn/). K-means clustering was performed using the Hartigan-Wong algorithm with 15 random starts. Temporal gene expression dynamics between RUG and MGT clusters were linked with Circos visualizations (https://circos.ca/). GO and KEGG enrichment analyses were performed based on the *V. vinifera* Ensembl GeneID alias, using the g: Profiler website with Benjamini-Hochberg multiple testing correction method ($P_{FDR} < 0.05$) (Kolberg et al., 2023). The pathways of the exclusive PB GO-terms of the cluster of interest were visualized by the Cytoscape plug-in ClueGO (Bindea et al., 2009).

2.10. Validation of DEG subsets by qPCR

DNase treatment, cDNA synthesis, and qPCR were conducted as described previously by Ismail et al. (2022). Gene-specific primers were designed with Primer Express v3.0 (Table S8). The qPCR reactions were performed using SsoAdvanced Universal SYBR Green Supermix (BIO-RAD Laboratories, Hercules, CA, USA). Each reaction was run in triplicate across three biological replicates on a CFX384 Touch Real-Time PCR Detection System (BIO-RAD Laboratories). Transcript levels were quantified through standard curves derived from serial dilutions of PCR products corresponding to each target and reference gene. The abundance was normalized against the stable reference genes *VvActin* and *VvEF1*. The geometric mean of these housekeeping genes was validated as an effective normalization factor.

2.11. Statistical analyses

Statistical analyses were conducted using multivariate ANOVA in IBM SPSS Statistics 22. Results were presented as mean ± SD from three independent replicates. Significant differences among treatments and genotypes were indicated by different letters, determined by Duncan's test at a significance level of $P < 0.05$.

3. Results

3.1. Physiological and anatomical characterization of grapevine rootstocks during drought

This study investigated the physiological and molecular responses of two grapevine rootstocks, RUG and MGT, with contrasting drought

resilience, focusing on their adaptation mechanisms during drought and recovery upon rehydration. Morphological comparisons between RUG and MGT reveal distinct differences in stomatal and leaf traits (Fig. S1). MGT has higher averages for stomatal density (12.8 ± 0.5) and stomatal size (29.3 ± 2.2 µm^2), as well as a larger leaf area (162.5 ± 13.7 cm^2). In contrast, RUG has significantly lower averages: stomatal density (10.8 ± 0.4), stomatal size (20.6 ± 1.2 µm^2), and leaf area (88.8 ± 5.5 cm^2) (Figs. S1A–C). A 7-day analysis of transpiration rates highlights the differing water management strategies of the rootstock genotypes (Fig. S1D). MGT maintains consistently higher transpiration rates, reaching a near-dry stage by day 3. Conversely, RUG exhibits slower transpiration rates, with water loss gradually increasing to levels comparable to MGT by day 6.

Gradual drought stress was applied to potted vines by withholding water until 35% SWC, after which rewatering was initiated. Leaf
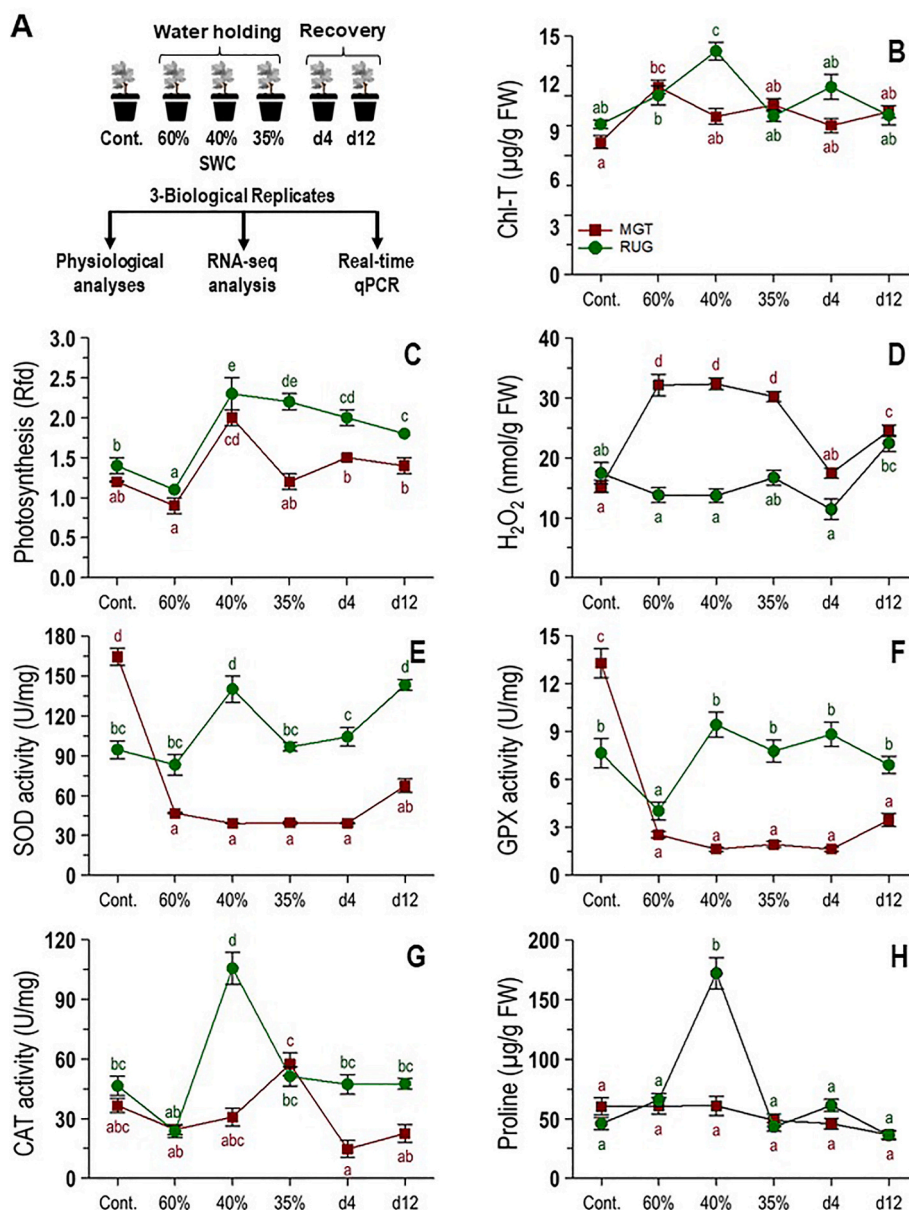
Fig. 1. Overview of the experimental procedure for drought induction and recovery phases. (A) The experimental setup utilized two grapevine rootstocks, Ruggeri 140 (RUG) and MGT-420A (MGT), selected for their contrasting drought response. Measurements were taken during water withholding and re-watering to assess (B) total chlorophyll content (Chl-T) and (C) the fluorescence decrease ratio (Rfd) in leaves. Panels (D–H) illustrated ROS-related parameters measured in both rootstocks, including (D) H$_2$O$_2$ levels, enzymatic activities of (E) superoxide dismutase (SOD), (F) glutathione peroxidase (GPX), and (G) catalase (CAT), as well as (H) proline content (Pro). Data represent means ± standard division (SD) of three biological replicates.

samples were collected at SWC levels of 60%, 40%, and 35%, as well as at 4 and 12 days after rehydration (d4 and d12). Regularly watered plants served as controls (Fig. 1A; Fig. S2). Sampling points were labeled chronologically: 1 - control, 2–60% SWC, 3–40% SWC, 4–35% SWC, 5 - day 4 post-rewatering, and 6 - day 12 post-rewatering. Under typical conditions, both rootstocks displayed similar basal levels of photosynthetic pigments (PhPs), particularly total chlorophyll (Chl-T) and chlorophyll-a (Chl-a), although RUG had significantly higher chlorophyll-b (Chl-b) levels (Fig. 1B; Figs. S3A and B). During drought, distinct patterns in PhP levels emerged, with RUG maintaining higher Chl-T and Chl-a levels at 40% SWC, which then dropped to initial levels at 35% SWC before stabilizing. MGT, however, struggled to accumulate these pigments and could not maintain them at 60% SWC (Fig. 1B; Fig. S3A). RUG showed slight increases in Chl-b at 40% SWC and on day 4 post-rewatering, significantly surpassing MGT levels (Fig. S3B). MGT's carotenoid levels plummeted at 60% SWC, despite being ~2.5 times higher than RUG's initially, which showed minimal variation in carotenoids throughout the experiment (Fig. S3C). While both rootstocks accumulated similar amounts of Chl-T and Chl-a at 60% SWC, only RUG continued to accumulate these pigments significantly at 40% SWC, enhancing its photosynthetic efficiency during drought and recovery, as indicated by fluorescence decrease ratio (Rfd) values (Fig. 1C). Interestingly, basal sugar levels did not correlate with initial PhPs and Rfd in either rootstock (Fig. S4). RUG leaves exhibited higher significant basal levels of monosaccharides; glucose (Glu) and fructose (Fru), but a non-significant total soluble sugar (TSS) compared to MGT leaves, which in contrast contained ~3 times more sucrose (Suc). During drought and rehydration, TSS accumulation patterns were similar, with some variation in sugar types.

To connect the differences in drought resilience between the rootstocks to their redox homeostasis, we monitored H_2O_2 content, antioxidant enzyme activities, and proline levels (Fig. 1D–H). H_2O_2, a stable ROS, doubled in MGT under drought compared to baseline levels, while RUG showed no increase (Fig. 1D). MGT managed to neutralize H_2O_2 to baseline levels after rewatering, indicating that drought was not severe enough to cause irreversible wilting. Additionally, MGT exhibited substantial declines in SOD and GPX activities (~3.5-fold and ~5.2-fold reductions, respectively), with slight recovery post-rewatering (Fig. 1E and F). In contrast, RUG maintained stable SOD levels throughout drought and recovery, showing notable increases at 40% SWC and 12 days post-rewatering (Fig. 1E). RUG also preserved GPX activity, with increases of ~2–~5.8-fold above MGT, except at 60% SWC, where it declined significantly (Fig. 1F). Proline levels and CAT activity sharply increased in RUG at 40% SWC, exhibiting ~3-fold elevation compared to other time points, while MGT only showed a minor CAT increase at 35% SWC (Fig. 1G and H).

The mortality rate was assessed using electrolyte leakage under PEG-induced stress conditions. In this experiment, eighteen grapevine rootstocks were evaluated by exposing leaf samples to a 10% polyethylene glycol (PEG) solution (Fig. 5A). PEG, a high molecular weight compound, does not penetrate cell walls and is widely utilized to induce osmotic stress in plant studies (Peiró et al., 2020). All grapevine rootstocks exhibited significant responses to the PEG treatment. The percentage of electrolyte leakage varied notably, ranging from 19.2% ± 1.3 for the RUG rootstock to 81.0% ± 3.5 for the MGT, demonstrating a substantial variability of 61.9% in drought resilience among the different grapevine genotypes. Additional assessments of drought tolerance focused on measuring the relative water content (RWC) in PEG-treated leaves of the two extreme rootstock genotypes, RUG and MGT. The RWC was quantified at 0, 6, 12, 24, and 48 h after treatment (Fig. S5B). While both rootstocks exhibited reductions in RWC under stress conditions, RUG demonstrated superior adaptability, whereas MGT exhibited a rapid decline in water content. The heightened sensitivity to water deficits observed in MGT may significantly affect its survivability in drought-prone environments.

Scanning electron microscopy (SEM) analysis revealed significant anatomical changes in drought-stressed grapevine rootstocks. In MGT, SEM identified two key features: (i) vessel occlusion by tyloses and (ii) starch granule accumulation in radial ray parenchyma cells (Fig. 2A and B). In contrast, RUG exhibited minimal starch buildup in cross and radial sections (Fig. 2C and D). Both rootstocks contained starch in axial and ray parenchyma cells, but MGT displayed greater starch accumulation, while RUG had fewer granules. Notably, tylose formation was exclusively observed in MGT, which is specific to this drought-sensitive rootstock (Fig. 2A–C).

Overall, these findings indicate that RUG possesses notable adaptability and robustness to drought, while MGT shows a pronounced sensitivity to water deficit conditions.

3.2. Transcriptomic changes during drought and recovery

To explore the molecular mechanisms of drought resilience, the transcriptome profiles of RUG and MGT rootstocks were analyzed during water deficit and recovery phases (Fig. 1A). The study generated 1.01 Gb of clean data with 20.88–37.18 Mb per replicate with mapping rates of 85.41%–91.77% (Fig. S6; Table S1). Hierarchical clustering revealed distinct transcriptomic shifts in both RUG and MGT in response to drought and recovery (Fig. S7). Principal Component Analysis (PCA) demonstrated high consistency among biological replicates, with clear sample separation across the two main components explaining 65% of the transcriptional variance (Fig. 3A). The first component (PC1) accounted for 45% of the variance, primarily attributed to drought and recovery effects, while the second component (PC2) represented 20%, mainly linked to rootstock genotype differences. Excluding recovery samples increased PC2 and decreased PC1, suggesting that each rootstock exhibited unique transcriptomic responses to both stress and recovery (Fig. S8). It was evident that drought stress emerged as the primary source of transcriptional variation, with rewatering further amplifying differences between the rootstocks.

To identify expressed genes during drought and recovery, RNA-seq data were analyzed using the DESeq2 R package with $P_{FDR} < 0.05$. Five pairwise comparisons were conducted within RUG (R2-R1, R3-R2, R4-R3, R5-R4, R6-R5) and MGT (M2-M1, M3-M2, M4-M3, M5-M4, M6-M5), yielding 11,313 and 14,436 non-redundant genes for RUG and MGT, respectively (Fig. 3B–D; Tables S2 and S3). Of these, 10,101 genes were commonly regulated, with 1212 and 4335 uniquely expressed in RUG and MGT, respectively (Fig. 3B). Within each rootstock, the distribution of up- and downregulated genes was approximately equal, particularly in RUG (Fig. 3C and D; Fig. S9). Recovery comparisons (M6-M5 and R6-R5) showed the highest transcriptional modulation, highlighting dramatic metabolic adjustments during recovery (Fig. 3C–F). To compare distinct transcriptional changes between RUG and MGT, each time point in RUG was aligned with its MGT counterpart (R–M). These pairwise comparisons revealed 13,765 unique transcripts, representing 43.2% of the *Vitis* transcriptome, confirming the impact of drought and recovery on PC1 variance (Fig. 4A; Table S4). The control comparison (R1-M1) identified the highest number of significantly redundant genes, followed by recovery comparisons (R5-M5 and R6-M6) and drought comparisons (R3-M3, R4-M4, R2-M2) (Fig. 4A; Table S4). In contrast, recovery comparisons had the most unique genes, consistent with PCA results (Fig. 3A; Fig. S10). Among the unique genes identified across comparisons, about 50% were common across three sets (within MGT, within RUG, and R-M) (Fig. S11). Comparing both rootstocks, regardless of drought or recovery, revealed 6112 unique genes constituting 19.2% of the *Vitis* transcriptome, confirming genotype as a source of PC2 variance (Fig. 3A). Approximately half of these were upregulated (2,688) or downregulated (3,424), with fewer exclusive genes (463) compared to other comparisons (Fig. 4B and C). These findings highlight extensive transcriptional reprogramming due to natural water deficit and rewatering.
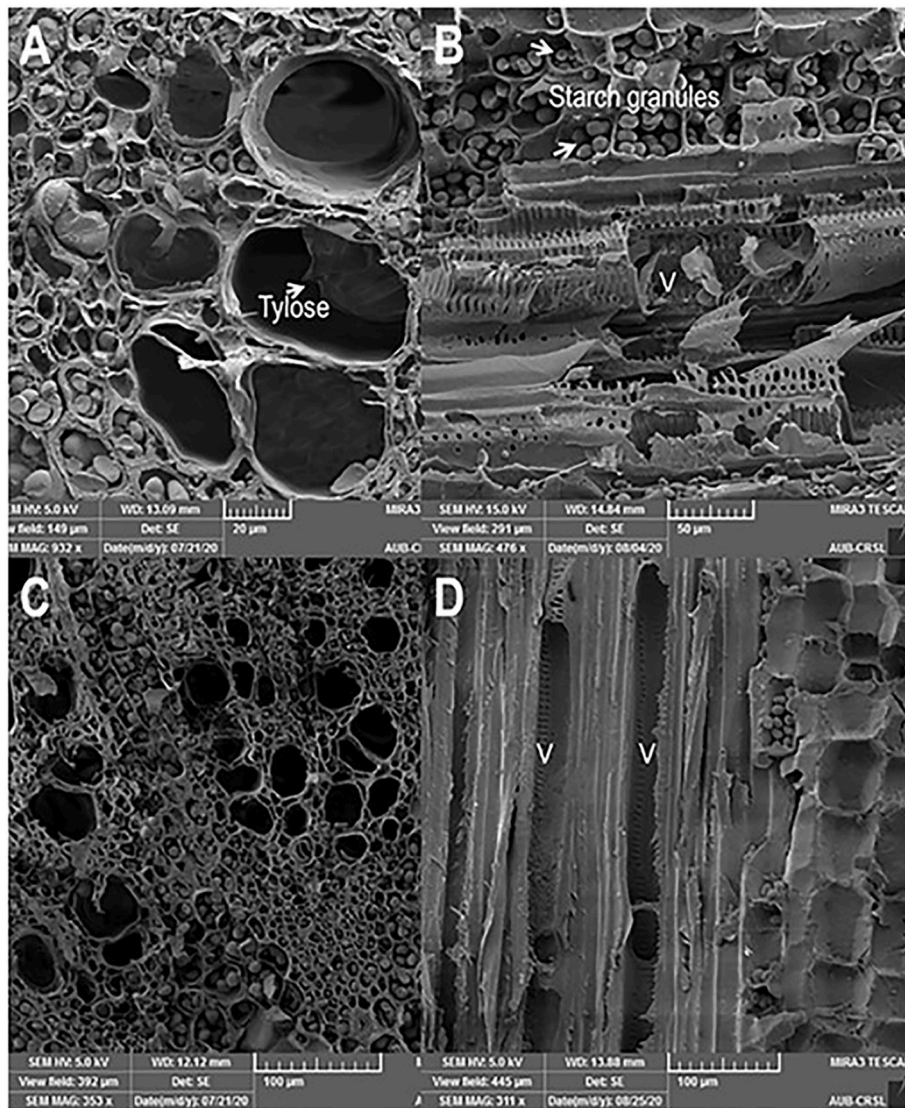
Fig. 2. Transverse and longitudinal radial sections of stem samples from MGT (A–B) and RUG (C–D) grapevine rootstocks grown under water deficit conditions (35% SWC). In MGT, vessel (V) occlusions with tyloses were evident in both transverse (A) and longitudinal (B) sections, impacting water flow as a response to drought stress. Abundant starch granules were visible in the xylem ray parenchyma cells, supporting potential energy storage for stress recovery. In contrast, the drought-tolerant RUG rootstock (C–D) exhibited no tylose formation, suggesting an adaptation to maintain hydraulic conductivity under stress, with only scattered starch granules observed in the xylem.

3.3. Cluster analysis reveals distinct transcriptional reprogramming during drought and recovery

Through the analyses, a total of 17,375 unique significant genes were identified in RUG and 17,390 in MGT, clustered into 15 groups based on their expression patterns during drought and recovery (Fig. 4D; Figs. S12–S14). For RUG, these clusters were reorganized into four groups reflecting their kinetic expression patterns (Fig. 4D; Fig. S13). Group I consists of drought-induced clusters (R-C1 to R-C5), with transcript levels peaking sequentially from the onset (R-C1) to the end (R-C5) of drought stress. Group II (R-C6 to R-C8) features clusters induced at various phases of both drought and recovery, indicating transient or recurring gene activation. Group III (R-C9 to R-C12) comprises clusters that remained stable or decreased during drought but increased during recovery, showing peaks at d4 and d12 (R-C9 and R-C10), only at d4 (R-C11), or solely at d12 (R-C12). In contrast, Group IV (R-C13 to R-C15) includes clusters with reduced transcript levels, either sharply (R-C13) or gradually (R-C14), or with a marked decrease following the control period (R-C15) (Fig. S13). These groups shed light on the temporal gene

expression dynamics linked to drought tolerance in RUG, highlighting potential targets for enhancing drought resilience. The MGT's clusters (M-C1 to M-C15) were similarly organized into four groups, reflecting the structure of RUG but with significant kinetic differences at specific time points, along with variations in gene identities and cluster sizes (Fig. 4D; Fig. S14). Notably, six clusters in RUG (R-C2, R-C3, R-C6, R-C7, R-C9, and R-C14) exhibited unique dynamic patterns without counterparts in MGT clusters (Fig. 4D; Figs. S13 and S14).

Furthermore, significant variation was detected among clusters and rootstocks across the three GO categories: Molecular Function (MF), Cellular Component (CC), and Biological Process (BP), as well as in KEGG pathways (Tables S6 and S7). For simplicity, our analysis focused on uniquely enriched BP GO terms, with special attention to the drought-tolerant RUG rootstock. In RUG, particularly the drought-specific cluster R-C3, many BP GO terms associated with drought adaptation were exclusively enriched, including "photosynthesis, light reaction", "monosaccharide biosynthetic process", "tetraterpenoid metabolic process", and "amino acid catabolic process" (Fig. 5B; Figs. S15–S19; Table S6). Conversely, the MGT-specific cluster M-C3
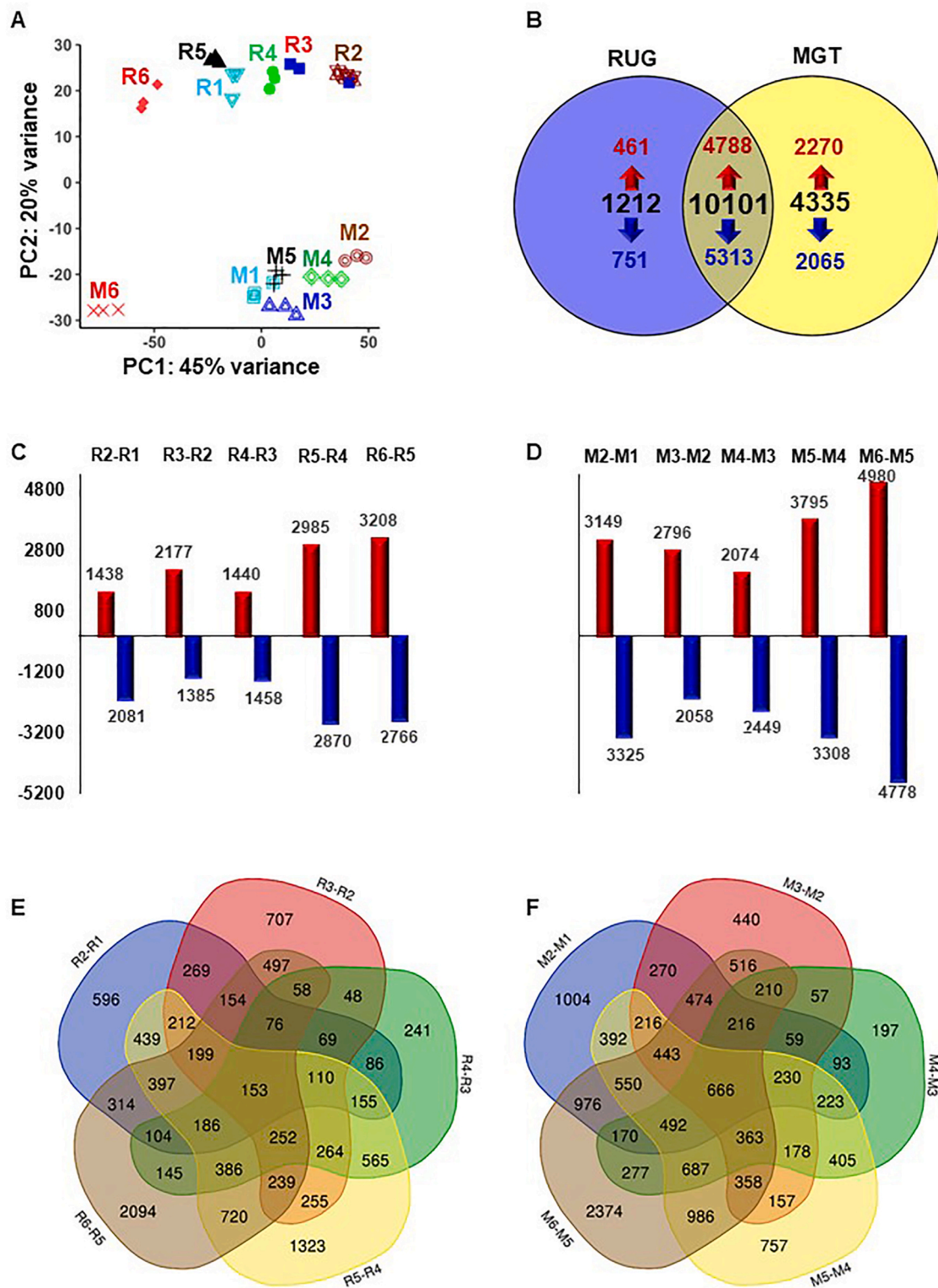
Fig. 3. Temporal dynamics of the Vitis transcriptome in RUG (R) and MGT (M) rootstocks during drought and re-watering. (A) Principal Component Analysis (PCA) illustrating the global transcriptomic similarities among RNA-seq replicates at each time point (sampling order 1–6: control, 60% SWC, 40% SWC, 35% SWC, day 4 post-rewatering, and day 12 post-rewatering). Each time point is represented by a unique color to track drought and recovery phases. (B) Differential expression analysis using the DESeq2 pipeline identified 11,313 and 14,436 unique differentially expressed genes (DEGs) in RUG and MGT, respectively (P$_{FDR}$ < 0.05). The Venn diagram displays the overlap and unique DEGs between rootstocks during drought and recovery. (C and D) Bar plots show significantly expressed genes between consecutive time points for RUG and MGT, respectively, totaling 21,808 and 32,711 DEGs (P-adjust <0.05). Upregulated and downregulated genes are represented by red and blue bars, respectively. (E and F) Venn diagrams highlight the overlap of significant DEGs across timepoint comparisons within each rootstock, providing insight into the distinct temporal gene expression patterns in response to drought and re-watering. (For interpretation of the references to color in this figure legend, the reader is referred to the Web version of this article.)
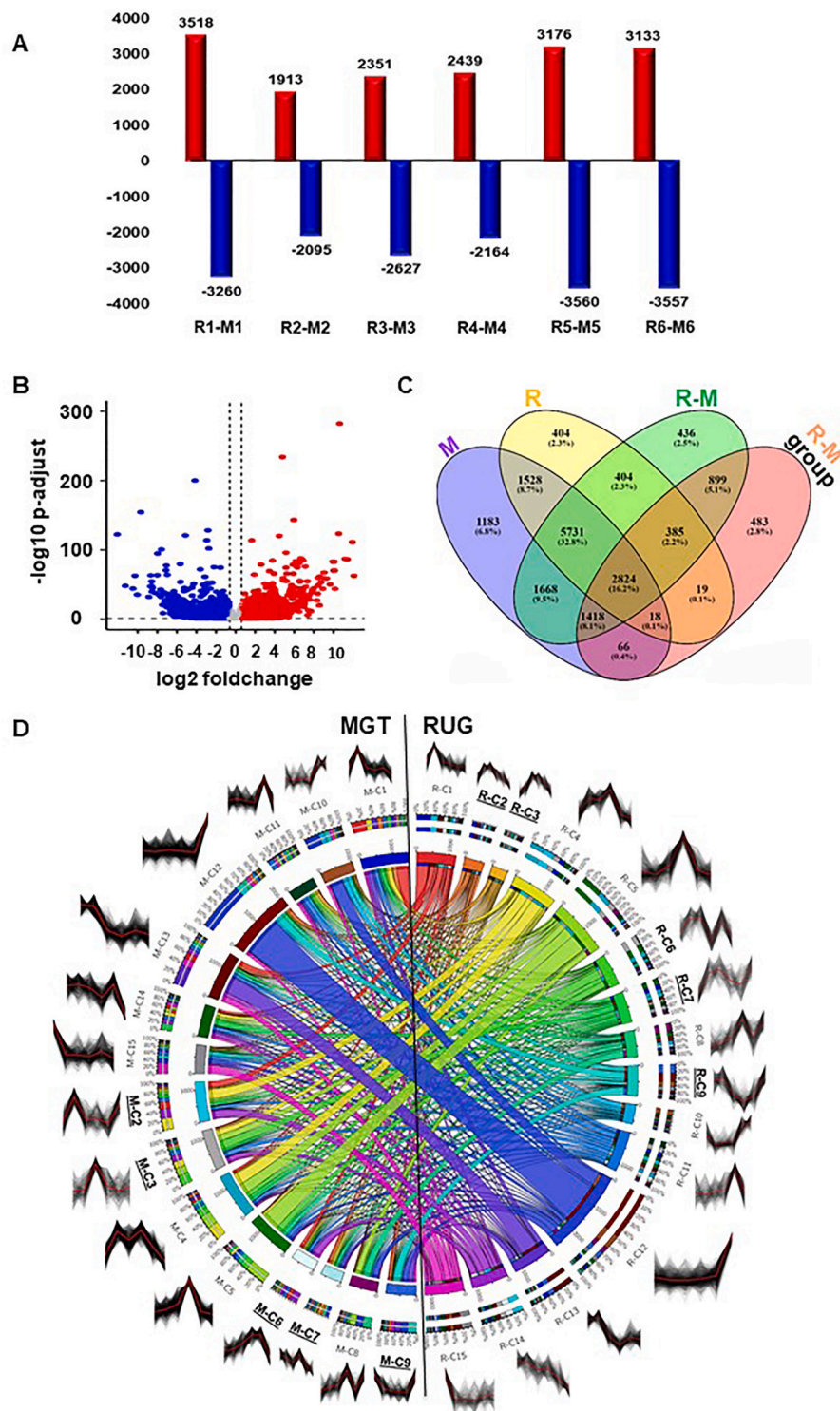
Fig. 4. Transcriptomic variance between RUG (R) and MGT (M) rootstocks during drought and re-watering. (A) Differential gene expression analysis comparing each time point in RUG against its corresponding time point in MGT (R–M) using the DESeq2 pipeline ($P_{FDR} < 0.05$). Sampling order 1–6 is as defined in Fig. 3. (B) Volcano plot displaying genes significantly upregulated (red), downregulated (blue), and non-expressed (grey) in RUG relative to MGT, capturing genotype-specific expression patterns irrespective of drought or re-watering phases. (C) Venn diagram illustrating non-redundant genes identified in four statistical comparisons: within RUG, within MGT, and between RUG and MGT, both across individual time points and as grouped treatments. (D) Clustering of genes from (C) using the K-means approach, grouped into 15 clusters (C1–C15) for RUG and MGT. The Circos plot visualizes relationships between corresponding clusters in RUG and MGT, highlighting transcriptomic distinctions between rootstocks under stress and recovery. (For interpretation of the references to color in this figure legend, the reader is referred to the Web version of this article.)

showed unique enrichment in three major drought adaptation networks: "response to inorganic substance", "regulation of stress response", and "regulation of cellular response to hypoxia" (Fig. 6B; Figs. S20–S24;

Table S7). The distinct dynamic patterns of cluster C3, as well as the variation in gene counts and identities between the two rootstocks, indicate that RUG achieved its drought resilience by expressing and

Fig. 5. Venn diagram illustrating the significantly enriched biological process (BP) GO terms within R-C3 and R-C5 K-means clusters from group I in the drought-tolerant rootstock, RUG. Network views display the major BP GO terms significantly enriched and unique to clusters R-C3 and R-C5, differentiating them from other clusters within RUG's first group. BP GO terms (*P*-adjusted <0.05) were extracted using the g: Profiler and mapped by the Cytoscape with ClueGO under default settings. Terms were functionally grouped by kappa score based on shared genes, with each group shown in distinct colors. Group names reflect the most significant term in each functional category. The size of the nodes indicates the number of mapped genes ranged from 0 to 5, 5–10, 10–20, 20–30, and ≥30 genes. (For interpretation of the references to color in this figure legend, the reader is referred to the Web version of this article.)

sustaining a higher number of tolerance-related genes during stress. Mapping BP GO in the C5 cluster supported this notion. Notably, several drought-related molecular networks were uniquely enriched in the RUG R-C5, e.g., "response to water deprivation", "carbohydrate metabolic process", "lignin metabolic process", "detection of brassinosteroid stimulus", "sulfur compound biosynthetic process", and "regulation of anatomical structure morphogenesis" (Fig. 5A; Fig. S19; Table S6). In contrast, the MGT M-C5 showed exclusive enrichment of the "mono-carboxylic acid metabolic process", "monosaccharide metabolic process", "carbohydrate catabolic process", "glucan metabolic process", "regulation of cellular component organization", and "starch catabolic process" (Fig. 6A; Fig. S24; Table S7). These findings underscore the distinct adaptive strategies employed by RUG and MGT, with RUG engaging a broader and more persistent set of drought-response pathways.

In the second group clusters, the RUG unique R-C6 displayed strong enrichment in several BP GO terms positively associated with stress response, such as "purine-containing compound catabolic process", "photosynthesis, light harvesting in photosystem I", "porphyrin-containing compound metabolic process", "thylakoid membrane organization", "cell redox homeostasis", and "cutin biosynthesis process" (Fig. 7B; Table S6). Conversely, the MGT unique M-C6 was significantly enriched with other stress-related BP GO terms like "monosaccharide metabolic process", "tetraterpenoid metabolic process", "folic acid-containing compound metabolic process", "carbohydrate metabolic process", and "regulation of cyclic-dependent protein serine/threonine kinase activity" (Fig. 7A; Table S7). Additionally, the BP GO term "generation of precursor metabolites and energy" was highly represented in both RUG R-C6 and MGT M-C6.

In the recovery-specific clusters (C9–C12), the C9 cluster exhibited significant enrichment of many RNA-related GO terms across both rootstocks. However, the MGT unique M-C9 displayed exclusive enrichment in gene networks associated with "mitochondrial calcium ion transmembrane transport" and "gametophyte development" (Fig. 8A; Table S7). In contrast, the RUG unique R-C9 showed distinct enrichment for gene networks such as "response to lipid", with several ABA-related GO terms, "endoplasmic reticulum to Golgi vesicle-mediated transport", "amine metabolic process", and "regulation of anthocyanin metabolic process" (Fig. 8B; Table S6). In Group IV, the MGT-specific M-C13 showed unique enrichment in gene networks like "glycolipid metabolic process" and "organelle disassembly" (Fig. 9A; Table S7). Conversely, the RUG-specific R-C13 displayed exclusive enrichment in networks including "cellular nitrogen compound metabolic process", "response to light stimulus", "photosynthesis, light harvesting in photosystem I", "tRNA metabolic process", "plastid organization", "carboxylic acid biosynthetic process", "organic acid biosynthetic process", and "porphyrin-containing compound metabolic process" (Fig. 9B; Table S6). Although various mitochondrial- and RNA-related GO terms were common in C13 of both rootstocks, significant differences were observed in their enrichment levels and number, a trend noted across other clusters as well.

In summary, our dataset provides valuable insights into the gene expression dynamics that govern drought response and recovery in these grapevine rootstocks. Notably, RUG exhibited a unique sequential induction pattern in Group I clusters, where distinct pathways were activated at different stages, maintaining upregulation in specific clusters to enhance drought resilience (Fig. S25). This adaptive expression dynamic was absent in MGT (Fig. S26), emphasizing that RUG holds a more robust drought-response strategy.

3.4. Validation of drought-dependent transcriptional changes

Our physiological and anatomical findings, alongside GO term analysis of transcriptomic data, revealed a complex interplay of various pathways influencing drought resilience in grapevine. Key pathways affecting resilience include photosynthesis, antioxidant mechanisms,

osmotic adjustments, and calcium signaling. To confirm the expression patterns of candidate genes involved in these pathways, qPCR analysis was performed from RNA samples used for RNA-seq libraries construction, along with two additional time points: 80% SWC and after 8 days post-recovery. The qPCR results showed strong consistency with transcriptomic data for both rootstocks, with correlation values exceeding $r^2 > 0.80$ and a significant p-value $<6.6 \times 10^{-5}$ (Fig. 10; Table S8).

RUG demonstrated higher expression across eight photosynthesis-associated genes involved in light energy acquisition and electron transport. Among these genes, *PETA* (photosynthetic electron transfer A) showed a remarkable increase in expression with drought progression, peaking at 4d post-rewatering (Fig. 10A). In RUG, *PETA* was upregulated by ~10- and ~11-fold at 40% and 35% SWC, respectively, compared to the control, which was ~27- and ~9-fold higher than corresponding values in MGT. This positions *PETA* as a key marker for photosynthetic efficiency and resilience under stress. Other key genes, including *CAB1* (chlorophyll A/B binding protein 1), *CBBL* (ribulose-bisphosphate carboxylase large chain), and several proteins from photosystems I and II, also showed strong induction in RUG, especially at 40% and 35% SWC, compared to MGT. *PsbC* (photosystem II reaction center protein C) was notably induced at 60% SWC in both rootstocks but later dropped below initial levels at 40% SWC, with RUG expressing ~2.7 times more transcripts than MGT under both stress and control conditions. Only RUG maintained elevated *PsbC* expression at 35% SWC, accumulating ~11-fold higher levels than MGT. During rewatering, RUG sustained steady *PsbC* expression, whereas MGT peaked at 4d post-rewatering before experiencing a second decline.

The antioxidant-related candidate genes were classified into two groups: antioxidant/stress signaling and antioxidant homeostasis. The antioxidant/stress signaling group includes 9 genes encoding redox-responsive transcription factor 1 (*RRTF1*), VQ motif-containing protein (*VQ*), and WRKY DNA-binding protein (*WRKY*). Notably, the expression of two *RRTF1* paralogs was suppressed to basal levels during early drought (80% and 60% SWC) in both rootstocks, partially recovering during severe drought events (40% and 35% SWC), especially in RUG. Both rootstocks showed increased *RRTF1* expression upon rewatering, indicating its recovery-related regulatory role. In contrast, *WRKY* genes displayed variable expression patterns, with higher levels mostly during the recovery phase. The three *VQ* paralogs exhibited clear drought-induced expression, particularly during severe drought incidents, with *VQ1* being upregulated ~3.6-fold and ~4.7-fold at 40% and 35% SWC compared to controls in both RUG and MGT (Fig. 10B).

The antioxidant homeostasis group comprised 34 genes associated with pathways involving ankyrin repeat family protein (*ANKRA*), oligopeptide transporter (*OPT*), peroxidase superfamily protein (*PRX*), terpene synthases (*TPS*), and UDP-glycosyltransferase superfamily proteins (*HYR1*) (Fig. 10C). This group showed significant upregulation in RUG compared to MGT, particularly at 40% and 35% SWC, with diverse expression patterns. For example, five of the six *ANKRA* genes in RUG exhibited drought-responsive patterns, peaking with increases of ~2–~6-fold at 35% SWC before gradually declining during rewatering. Similarly, the expression of three *OPT* genes in RUG rose during drought, particularly at 35% SWC, but declined during recovery, while MGT showed earlier *OPT* expression at 60% SWC and after 4d of recovery. The *PRX2* mRNA responded to drought in both rootstocks, with RUG accumulating ~4 times more transcripts than MGT at 35% SWC. The *TPS* genes in RUG were markedly upregulated at both 60% and 40% SWC, while MGT had limited *TPS* transcription, with minimal induction observed. Likewise, *HYR1* expression in MGT was weak, with three out of twelve genes showing a noticeable increase (~8- to ~42-fold) by day 12 of recovery. In contrast, *HYR1* genes in RUG were generally active, with seven out of twelve genes showing strong expression at 40% or 35% SWC, maintaining high levels throughout the recovery phase. Calcium-related genes also displayed distinct expression patterns among rootstocks (Fig. 10D). For instance, *CAL3* was significantly abundant in RUG during drought stress, particularly at 40% SWC, indicating a more
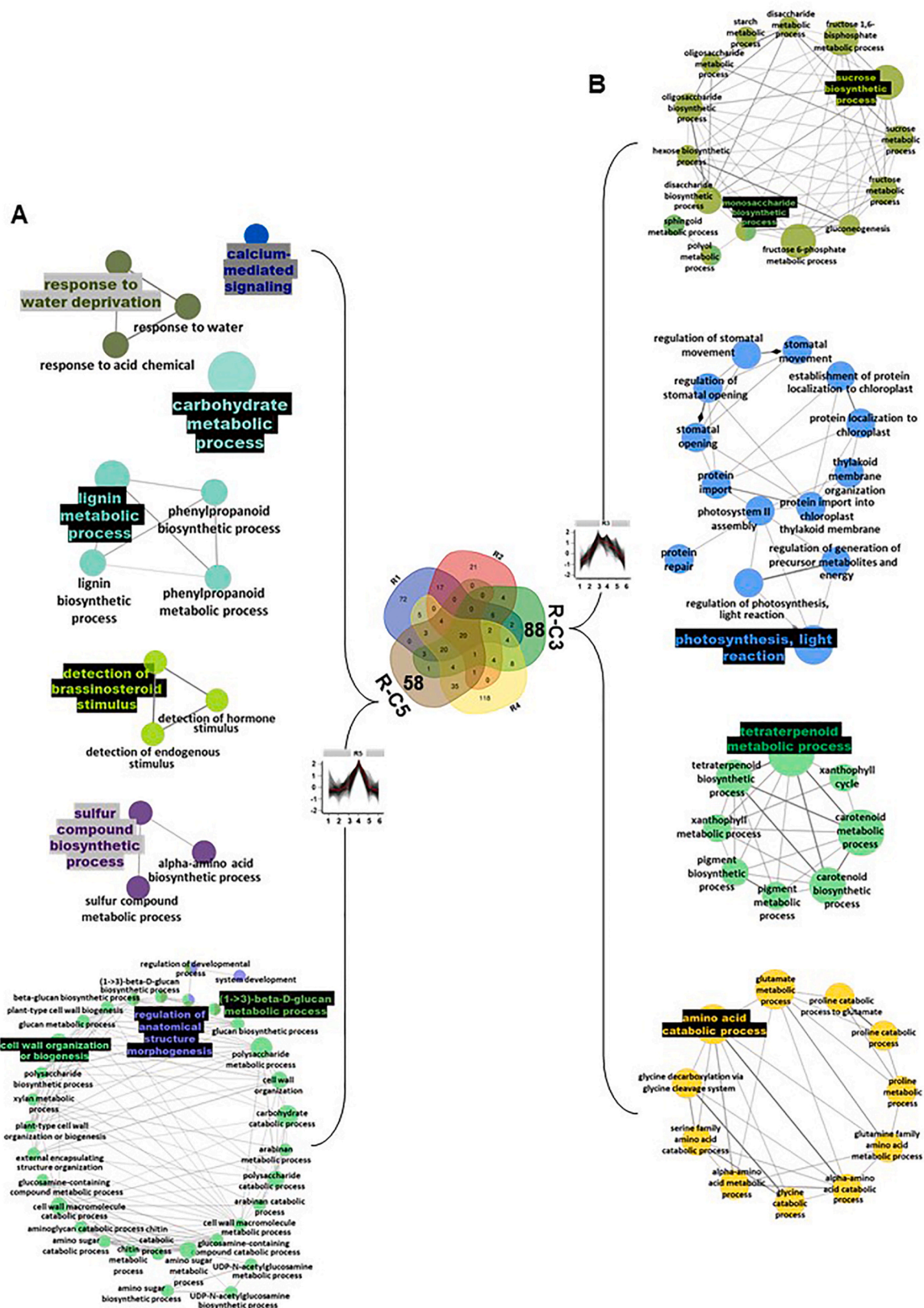
Fig. 6. Venn diagram illustrating the significantly enriched biological process (BP) GO terms within M-C3 and M-C5 K-means clusters from group I in the drought-sensitive rootstock, MGT. Network views highlight the major BP GO terms that are significantly enriched and unique to clusters M-C3 and M-C5, setting them apart from other clusters within MGT's first group. BP GO terms (*P*-adjusted <0.05) were extracted using the g: Profiler and mapped by the Cytoscape ClueGO plugin under default settings. Terms were functionally grouped by shared genes using kappa scores, with distinct colors representing each group. The most significant term names each functional category. The size of the nodes indicates the number of mapped genes ranged from 0 to 5, 5–10, 10–20, 20–30, and ≥30 genes. (For interpretation of the references to color in this figure legend, the reader is referred to the Web version of this article.)
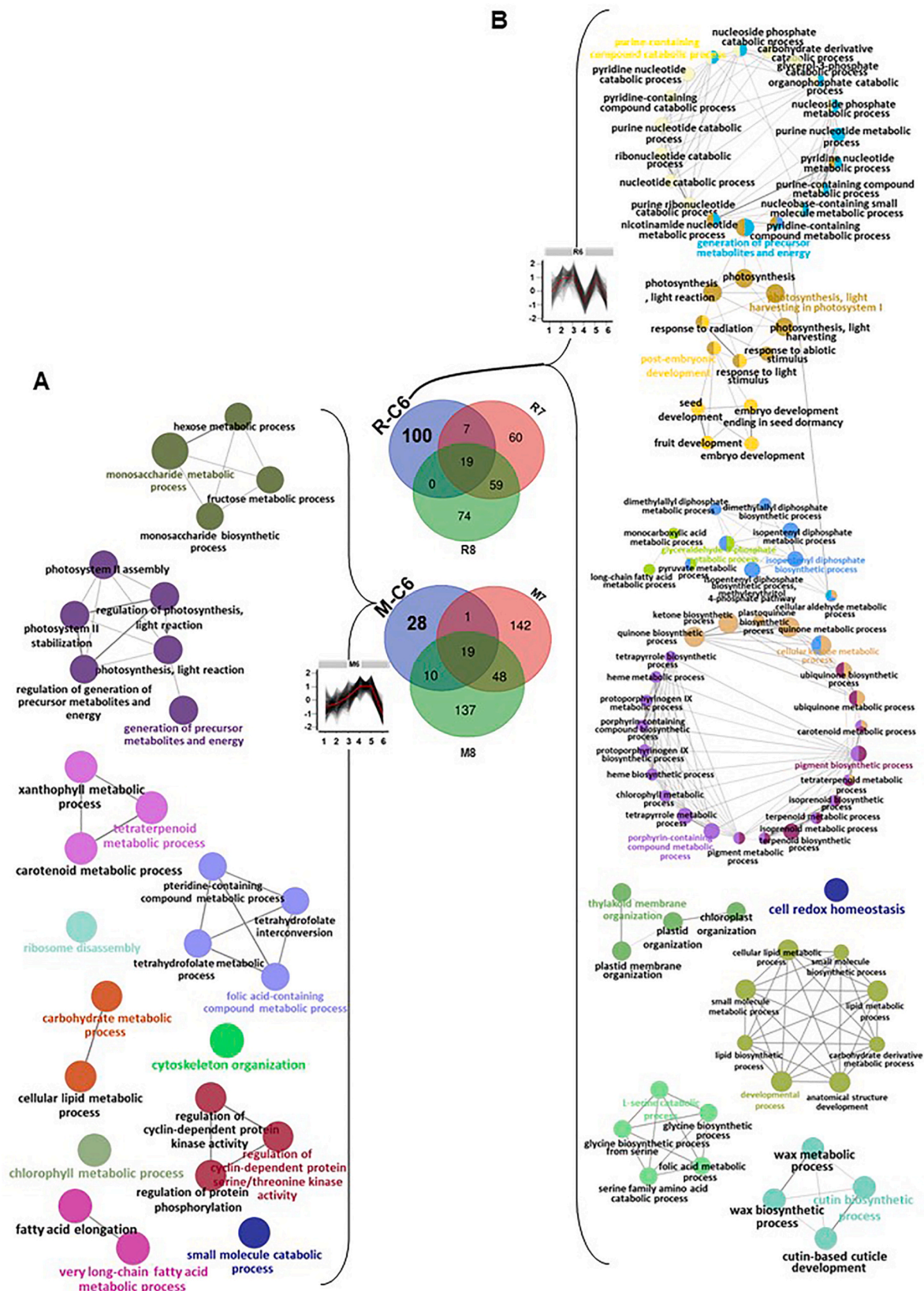
Fig. 7. Venn diagram highlighting the significantly enriched biological process (BP) GO terms within the C6 K-means cluster for both drought-sensitive (MGT) and -tolerant (RUG) rootstocks. Network views display the key BP GO terms uniquely enriched in M-C6 and R-C6 clusters for MGT and RUG, respectively, distinguishing them from other clusters in each rootstock's second group. BP GO terms (*P*-adjusted <0.05) were extracted by the g: Profiler and mapped by the Cytoscape ClueGO plugin under default parameters. Terms were functionally grouped by shared genes with kappa scores, with distinct colors representing each group, and the most significant term names each functional category. The size of the nodes indicates the number of mapped genes ranged from 0 to 5, 5–10, 10–20, 20–30, and ≥30 genes. (For interpretation of the references to color in this figure legend, the reader is referred to the Web version of this article.)
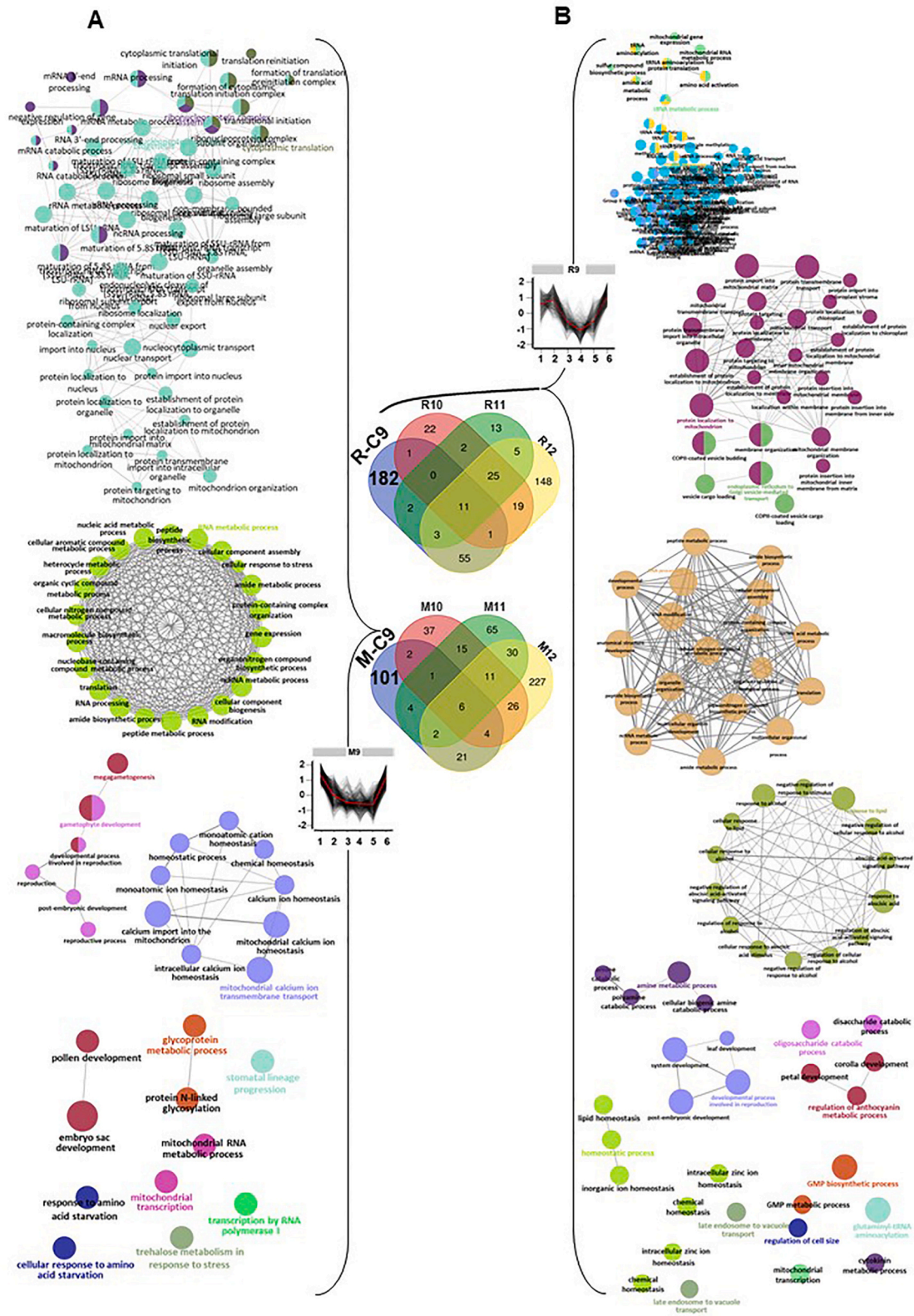
Fig. 8. Venn diagram depicting the significantly enriched biological process (BP) GO terms within the K-means cluster 9 for both drought-sensitive (MGT) and -tolerant (RUG) rootstocks. Network views illustrate the major BP GO terms uniquely enriched in clusters M-C9 (MGT) and R-C9 (RUG), distinguishing these from other clusters within the third group of each rootstock. BP GO terms (*P*-adjusted <0.05) were extracted by the g: Profiler and mapped by the Cytoscape ClueGO plugin under default settings. Terms were functionally grouped by shared genes with kappa scores, with distinct colors representing each group, and the most significant term serving as the group label. The size of the nodes indicates the number of mapped genes ranged from 0 to 5, 5–10, 10–20, 20–30, and ≥30 genes. (For interpretation of the references to color in this figure legend, the reader is referred to the Web version of this article.)
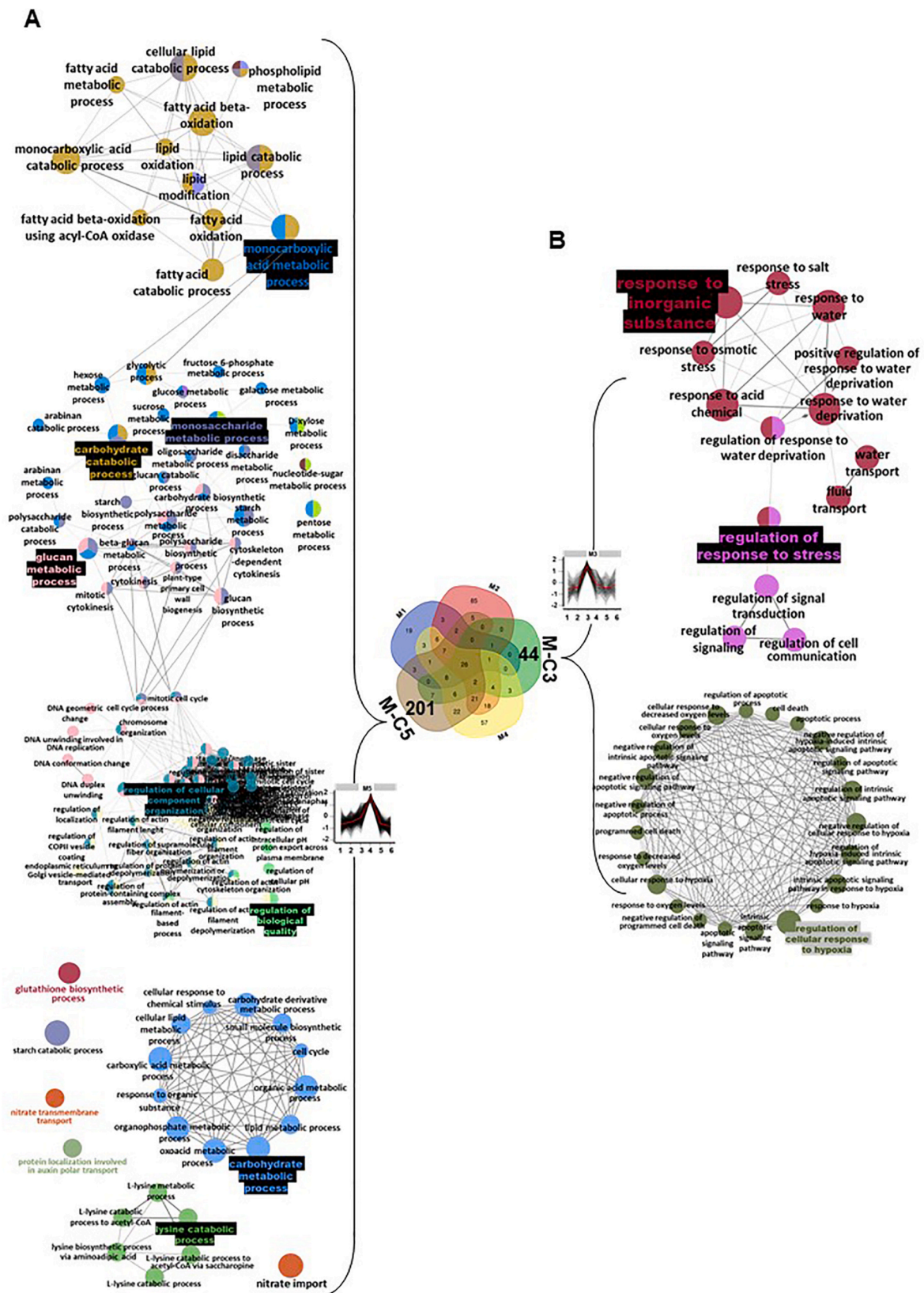
Fig. 9. Venn diagram illustrating the significantly enriched biological process (BP) GO terms within the C13 K-means cluster for both drought-sensitive (MGT) and -tolerant (RUG) rootstocks. Network views highlight the major BP GO terms uniquely enriched in clusters M-C13 (MGT) and R-C13 (RUG), with these terms exclusively represented in each cluster compared to other clusters within the fourth group of each rootstock. BP GO terms (*P*-adjusted <0.05) were extracted by the g: Profiler and mapped by the Cytoscape ClueGO plugin, using default settings. Terms were functionally grouped by shared genes with kappa scores, with distinct colors representing each group, and the most significant term was used to label each group. The size of the nodes indicates the number of mapped genes ranged from 0 to 5, 5–10, 10–20, 20–30, and ≥30 genes. (For interpretation of the references to color in this figure legend, the reader is referred to the Web version of this article.)

Fig. 10. Heatmap showing the expression profiles of 81 hub genes significantly regulated during drought and/or re-watering in RUG and MGT rootstocks, using the qPCR approach. Sampling times were labeled sequentially as 1 through 6, corresponding to control, 60% SWC, 40% SWC, 35% SWC, day 4 post-rewatering, and day 12 post-rewatering, respectively. Two additional sample time points were added, including 80% SWC and day 8 post-rewatering, denoted by '+' and '++,' respectively. For gene abbreviations and additional details, refer to Supplementary Table S8.

robust response than in MGT.

The RUG-Up gene group exhibited a rootstock-specific abundance pattern in RUG during drought and recovery phases, including osmotin 34 (*OSM34*, 5 paralogs), phosphate transporter 1 (*PHT1*, 2 paralogs), ABC-type transporter family protein (*ABC2*), β-glucosidase 11 (*BGlu11*), sucrose-phosphate synthase family protein (*SPS4*), β-hexosaminidase 3 (*BHEX*), and chalcone synthase family protein (*CHS*) (Fig. 10E). For instance, *OSM34* genes initially declined under stress in both RUG and MGT but later spiked significantly at 35% SWC or at 12 days of

rewatering, a pattern much more pronounced in RUG, suggesting that RUG is more reliant on *OSM34* and associated genes for drought adaptation and recovery. On the contrary, the MGT-Up gene group consists of genes e.g., cellulose synthase (*CS*, 3 paralogs), FASCICLIN-like arabinogalactan family protein (*FLA*, 4 paralogs), RALF-like 33 (*RLF33*), senescence-related gene 1 (*SRG1*), the nodulin MtN21/EamA-like transporter family protein (*UMAMIT*), and blue-copper-binding protein (*BCB*) (Fig. 10F). These genes are preferentially expressed in MGT during drought and rewatering, whereas their expression in RUG was

generally downregulated or absent.

Overall, RUG leaves exhibited an upregulation of a variety of transcripts that contributed to maintaining better osmotic and redox homeostasis during drought stress, with this balanced response extending into the recovery phase. This suggests that the RUG gene expression patterns are more robustly tuned toward protecting cellular integrity through consistent antioxidant activity and stress signaling pathways, supporting resilience and recovery after drought conditions. This regulated osmotic and redox homeostasis likely played a key role in the ability of RUG to be osmotically adjusted and to prevent/mitigate oxidative damage and maintain functional metabolic activity, distinguishing its drought tolerance strategy from that of MGT.

4. Discussion

4.1. RUG maintains high osmotic and redox homeostasis efficiency during drought

Plants have developed a complex antioxidant defense system to regulate reactive oxygen species (ROS), thereby minimizing their potentially harmful effects (Mittler et al., 2022). Water scarcity significantly impairs photosynthesis by elevating ROS levels, which negatively impact crucial enzymes such as Rubisco and ATP synthase located in chloroplasts (Lawlor and Tezara, 2009; Pinheiro and Chaves, 2011). As a primary site of ROS production, chloroplasts depend on robust redox regulation mechanisms to modulate physiological responses and sustain photosynthetic efficiency under stress (Moreno et al., 2008). Stomatal closure, an adaptive response designed to reduce water loss, restricts CO_2 diffusion into chloroplasts, subsequently diminishing Rubisco activity and limiting photosynthesis (Flexas et al., 2006; Hasanuzzaman et al., 2023; Madumane et al., 2024). In response, stress-tolerant plants employ various antioxidant defenses, with the drought-stressed hybrid RUG demonstrating enhancements in this regard. RUG, identified as one of three drought-tolerant hybrids of *V. berlandieri* × *V. rupestris*, exhibits superior photosynthetic performance and efficient water usage even under severe water limitations (Bianchi et al., 2020). SOD serves as a primary defense by converting superoxide anions (O^{2-}) into oxygen (O_2) and hydrogen peroxide (H_2O_2), which are subsequently detoxified by enzymes like GPX, CAT, and ascorbate peroxidase (APX) to yield water (Apel and Hirt, 2004). While most antioxidant enzymes are distributed across various cellular compartments, CAT is primarily located in peroxisomes (Cruz de Carvalho, 2008). The increased activity of CAT in RUG highlights its critical function in mitigating ROS accumulation during periods of water deficit. This adaptive response aligns with a critical threshold of stress severity indicated by PhPs measurements, while under salinity, RUG did not show a significant increase in CAT activity contrasting with MGT, which exhibited a slight increase after salt exposure (Gajjar et al., 2023). The accumulation of Pro in RUG parallels the increase in CAT, emphasizing the need for synergistic ROS mitigation strategies during prolonged drought. Both RUG and MGT displayed elevated levels of Pro following salinity exposure, equivalent to the RUG Pro response to drought. Pro functions as a potent antioxidant, accumulating intracellularly in response to abiotic stressors. It acts as an osmoprotectant, stabilizing proteins and membranes while scavenging ROS, thereby enhancing stress resilience (Ghosh et al., 2022). In chloroplasts, elevated Pro levels facilitate stress adaptation by buffering $NADP^+$ as an electron acceptor, thereby protecting photosynthetic systems from damage induced by superoxide ($O_2^{\bullet-}$) and shielding thylakoid membranes from oxidative injury (Rehman et al., 2021; Hosseinifard et al., 2022). Furthermore, Pro is transported to roots, promoting cellular homeostasis and osmotic balance (Wang et al., 2022). This transport strategy may benefit RUG during drought and recovery, in stark contrast to MGT, which experienced drought-induced anatomical changes such as starch granules accumulation and tylose occlusions in vessels. Excessive tylose formation can block xylem parenchyma cells, consequently reducing hydraulic conductivity (Sun et al., 2013; Ingel

et al., 2020). In instances of drought-induced xylem cavitation or pathogen-related occlusions, xylem vessels lose hydraulic function as they fill with air, tylose, or gels, leading to wilting and potentially compromising plant survival (Pouzoulet et al., 2019). In grapevines, prolonged water stress intensifies tension within the water column, causing embolisms that disrupt xylem vessel function, potentially resulting in hydraulic failure, leaf drop, and vine decline (Gambetta et al., 2020). The accumulation of starch granules in drought-sensitive MGT indicates an adaptive physiological strategy to cope with water deficits. This phenomenon suggests that the plant may enter a state of para-dormancy, where growth is suppressed due to ineffective stress alleviation. Starch acts as a crucial energy reserve, and its buildup often signals a shift in metabolic priorities under stressful conditions. Several studies indicated that solute release from starch granules into xylem conduits contributes to creating an osmotic gradient, facilitating water refilling in embolized vessels, and thus supporting survival during prolonged drought (Cochard et al., 2010; Nardini et al., 2011; Brodersen and McElrone, 2013). Despite moderate drought treatments allowing MGT to evade permanent wilting, the late accumulation of starch limits its effectiveness as a preventive defense mechanism. Conversely, RUG exhibits a more resilient strategy, promptly coordinating redox homeostasis and osmotic adjustments to fend off adverse drought effects. These tightly regulated mechanisms operate synergistically with other adaptive responses to protect critical biological processes like photosynthesis and maintain hydraulic conductance during drought stress.

4.2. Transcriptomic insights into drought resilience

Resilience differences between the drought-sensitive MGT and drought-tolerant RUG during water deficit and recovery highlight distinct molecular events that contribute to rapid resilience versus delayed recovery or potential vine mortality. Both rootstocks exhibited a general decline in gene expression during drought, which rebounded during rewatering. Comparative analysis confirmed that MGT experienced substantial gene downregulation as it transitioned to drought, followed by upregulation during recovery. This suggests that resilience is shaped not only by the dynamic transcriptomic and metabolic shifts during stress and recovery but also by the foundational transcriptomic state of the rootstock before stress. PCA analysis highlighted significant shifts in the grapevine transcriptome throughout stress and recovery, illustrating the divergence between MGT and RUG and emphasizing the influence of both pre- and post-stress events on drought resilience. Clustering analysis of the *Vitis* transcriptome profiles identified six distinct clusters out of fifteen that exhibited exclusive dynamics in each rootstock. These clusters were organized into five categories based on gene expression kinetics during drought and recovery. Notably, Group I displayed a sequential induction of gene expression in RUG primarily under stress, representing core elements of its drought resilience transcriptome. Mapping the GO terms and KEGG pathways of this group revealed RUG-specific enrichment in several molecular networks associated with drought resilience. Particularly, clusters that progressed with increasing drought severity, included pathways such as "photosynthesis, light reaction", "tetraterpenoid metabolic process", and "amino acid catabolic process". These processes facilitate photosynthetic stability, osmotic adjustment, and structural remodeling, reflecting RUG's adaptive response to drought. In contrast, resilience-related networks in MGT, such as "regulation of response to stress" and "cellular response to hypoxia" (cluster M-C3), were less responsive and activated at 40% SWC, while clusters linked to "vesicle-mediated transport" and "starch metabolism" peaked at 35% SWC, likely to address drought-induced damage and support the hypothesis of a vesicle repair mechanism. This contrasts with the rapid and robust responses in RUG, suggesting a more effective resilience strategy. Overall, the data illustrate that RUG responds dynamically to dehydration, with sequential activation of numerous stress-related genes that collectively mitigate drought effects.

Most genes within the three clusters of Group II were associated with physiological processes that occur during drought stress and recovery. For example, the R-C6 genes exhibited sharp downregulation under severe drought and at d12 of rewatering, yet these genes showed significant enrichment in molecular networks that enhance plant performance during drought, including the "tetrapyrrole metabolic process" (Nagahatenna et al., 2015). Tetrapyrroles, including chlorophyll, siroheme, heme, and phytochromobilin, share a common biosynthetic pathway localized in plastids (Tanaka et al., 2011). These macrocyclic organic tetrapyrroles, particularly porphyrins, have been linked to enhanced drought tolerance in transgenic rice (Phung et al., 2011). The substantial enrichment of molecular networks related to photosynthesis, cell redox homeostasis, cutin biosynthesis, and thylakoid membrane organization within R-C6 underscores the synergistic effects of various gene sets that enhance biological processes also present in R-C3 and R-C5, though with different kinetic responses. In contrast, the stress-related pathways in the M-C6 cluster were associated with metabolic processes involving carbohydrates, monosaccharides, and tetraterpenoids. During the recovery phase, both rootstocks displayed significant enrichment in RNA-related GO terms (C9), indicating a shift in metabolism toward growth rather than stress defense. However, the distinct molecular signatures of these events varied significantly between the two rootstocks, as evidenced by the enriched GO terms across all clusters in Group III. The decline kinetics observed in Group IV clusters illustrated the adverse effects of drought and, to a lesser extent, rewatering on a wide array of molecular pathways in both rootstocks, including mitochondrial and RNA-related processes, albeit with differing kinetics and enrichment levels. For instance, biological processes related to porphyrin metabolism were prominently featured in the R-C13 cluster, while similar processes appeared in different clusters for MGT. Our data provide detailed valuable insights into the molecular events occurring during stress and recovery in RUG and MGT, emphasizing transcriptomic shifts alongside physiological and anatomical adaptations. This affirms the superior resilience mechanisms in RUG and suggests opportunities for developing the next generation of stress-tolerant genotypes.

4.3. Integrating transcriptomic responses to stress with osmotic and redox homeostasis

This study identifies key stress biomarker genes, emphasizing the modulation of photosynthesis-related genes. Notably, RUG exhibits a superior ability to maintain and restore gene expression under severe drought circumstances compared to MGT. Protecting photosynthesis is essential for converting solar energy into sugars required for plant growth (Smeekens, 2000; Yang et al., 2020). Drought can hinder this process by affecting the biochemical status of chloroplasts and inducing stomatal closure (Hsu et al., 2020). Stomatal movement is regulated by intricate signaling pathways, with Ca^{2+} and ABA playing fundamental roles (Mishra et al., 2006).

Under osmotic stress, hydraulic signals from roots trigger ABA biosynthesis in leaves, utilizing both *de novo* synthesis and the recycling of glucose-conjugated ABA (ABA-GE) (Wang et al., 2020). The ABA recycling is facilitated by β-glucosidases, a multigene family essential for various cellular processes, including cell wall remodeling and lignification (Warzecha et al., 2000; Ahn et al., 2010). For instance, a rice mutant lacking the chloroplast-localized β-glucosidase *Os3BGlu6* displayed dwarfism, increased drought sensitivity, reduced ABA levels, diminished photosynthesis rates, and elevated intercellular CO_2 levels (Wang et al., 2020). Other studies indicated that β-glucosidases from *Arabidopsis* and barley can convert ABA-GE into free ABA in the leaf apoplast (Dietz et al., 2000; Lee et al., 2006). Consistent with these findings, RUG showed a significant increase in *βGLU11* transcripts during drought, indicating that the expression of *PETA* and *βGLU11* serves as biomarkers for stress resilience.

Additionally, ROS signaling and osmolyte synthesis during drought

are closely tied to ABA (Das and Roychoudhury, 2014; Park and Kim, 2021). The abundance of osmotin, a multifunctional stress-responsive pathogenesis-related (PR)-5 protein, is driven by ABA in response to various abiotic stresses, facilitating plant adaptation (Raghothama et al., 1997; Anil Kumar et al., 2015). In Arabidopsis, the *osm34* deletion mutant exhibited lower ABA sensitivity and proline levels (Park and Kim, 2021). Notably, *OSM34* abundance significantly increased during severe drought and rewatering in RUG compared to MGT. Drought stress leads to osmotic disturbance and loss of turgor pressure; therefore, drought-tolerant plants synthesize organic solutes like proline and glycine to restore osmotic balance (Kim et al., 2024). This osmotic adjustment is further supported by phosphate homeostasis through the induction of phosphate transporter genes (*PHT1 - 5*) in apples (Sun et al., 2017) and sucrose biosynthesis via sucrose phosphate synthase (*SPS*) in tomato (Duan et al., 2021). Moreover, the accumulation of flavonoids and phytoalexins, enhanced by CHS expression, along with the formation of flavonoid aglycones catalyzed by β-glucosidase (*BGLU*), further contribute to this osmotic adjustment (Dao et al., 2011; Du et al., 2024).

Maintaining redox homeostasis is crucial for resilience mechanisms. Consequently, we focused on genes related to redox homeostasis that were upregulated during stress and recovery, especially in RUG. The data indicated that half of the ROS-related proteins (21 genes) are in Group I clusters, compared to only 12 in MGT. Although these genes are dispersed across numerous cellular processes, they are integral to redox homeostasis. *RRTF1*, a transcription factor regulated by redox signals from the photosynthetic electron transport chain, is systemically upregulated by abiotic stress-induced redox signals (Khandelwal et al., 2008; Matsuo and Oelmüller, 2015). Transgenic *Arabidopsis* lines overexpressing *RRTF1* showed over 800 genes upregulated, with ~40% linked to stress response, redox balance, cell death, and senescence (Matsuo et al., 2015). However, the specific mechanisms by which *RRTF1* regulates redox homeostasis and facilitates plant adaptation to oxidative stress remain elusive (Matsuo and Oelmüller, 2015).

The substantial upregulation of genes related to VQ motif-containing proteins, ankyrin repeat proteins, terpene synthases, and UDP-glycosyltransferases during severe water scarcity in RUG supports its drought resilience. VQ proteins are essential for growth, development, and abiotic stress responses (Yuan et al., 2021). Overexpressing *TaVQ4-D* in *Arabidopsis* and *wheat* improved drought tolerance via upregulating ROS-scavenging genes and increasing SOD activity and proline content while reducing malondialdehyde (MDA) levels (Zhang et al., 2023). Conversely, silencing *TaVQ4-D* resulted in the loss of these beneficial traits. Furthermore, higher transcript levels of *PRX2* and *ANKRA3*, encoding class III peroxidases and ankyrin repeat proteins, respectively, were linked to increased antioxidant activity in RUG. In soybeans, overexpressing *GmANK114* boosted proline levels and reduced MDA content while decreasing H_2O_2 and O^{2-} accumulation during stress (Zhao et al., 2020).

In contrast, MGT exhibited transcriptional changes regulating cell wall components, including cellulose synthase (*CS*) and FASCICLIN-like arabinogalactan proteins (*FLAs*), during stress. FLAs are structural glycoproteins mainly localized in xylem tissues, vital for cell wall development (Zhang et al., 2015; Ma et al., 2023). The transcript levels of *FLAs* in poplar significantly correlate with wood fiber properties and cellulose microfibril orientation (Lafarguette et al., 2004). In *Arabidopsis*, *FLA11* and *FLA12* influence stem properties by altering cellulose deposition and impacting the integrity of the cell wall matrix (MacMillan et al., 2010). In tomato, *FLA1* and *FLA3* increased significantly in response to drought and hormone treatments, including MeJA and ABA (Yao et al., 2023). The upregulation of *FLAs* and *CS* in MGT during rewatering suggests their crucial roles in cell wall synthesis and remodeling during stress relief.

5. Conclusion

Plants can exhibit various environmental adaptations, with plasticity

Fig. 11. Proposed model summarizing drought resilience mechanisms in RUG. Drought conditions initiate cellular damage events, including ROS surges and osmotic imbalance, which are mitigated in RUG through strong redox and osmotic homeostasis. At the molecular level, RUG exhibits sequential induction of drought-responsive gene expression enriched in networks associated with resilience. Key processes contributing to this resilience include pathways supporting photosynthetic stability (e.g., R-C3's BP GO term "photosynthesis, light reaction"), osmotic regulation (e.g., R-C3's BP GO term "amino acid catabolic process"), and structural adaptation (e.g., R-C5's BP GO terms "lignin metabolic process" and "regulation of anatomical structure morphogenesis"). The size of the nodes indicates the number of mapped genes ranging from 0 to 5, 5–10, 10–20, 20–30, and ≥30 genes, while the color indicates each group with the most significant term defining the name of the group. Additionally, upregulation of various stress-related genes reduces oxidative stress, leading to elevated antioxidant activities (SOD, GPX, and CAT) and increased proline (Pro) accumulation in RUG cells. This response helps maintain ROS (e.g., H_2O_2) at controlled levels. Pro, likely along with other osmolytes, is also essential for RUG's osmotic balance under stress, as evidenced by healthy xylem structure. This osmotic adjustment is reflected in RUG's enhanced photosynthetic efficiency during severe drought and recovery, indicated by an improved fluorescence decrease ratio (Rfd). (For interpretation of the references to color in this figure legend, the reader is referred to the Web version of this article.)

playing crucial roles in ecosystems, agriculture, and aesthetics. Our research suggested that grapevines can rebuild their defense mechanisms and restructure systems to maintain productivity during water scarcity. Grapevines perceive stress signals, triggering changes in growth behavior and employing defense mechanisms, such as antioxidant scavenging, osmo-protection, and osmotic adjustment, enabling flexible growth modulation during environmental changes. While all vines possess components for drought tolerance, the key difference lies in their responsiveness to stress. Comparative analysis revealed that RUG harbors a conservative water-use strategy essential for water retention. Conversely, MGT is better suited for conditions favoring vigor growth with higher transpiration and photosynthetic efficiency. This study emphasizes redox and osmotic homeostasis as key mechanisms driving drought resilience grapevine. The proposed model (Fig. 11) illustrates how RUG maintains a strong redox and osmotic balance, enabling it to prevent or effectively mitigate drought-related disruptions. Under drought, RUG showed a sequential induction of gene expression, enriching resilience-associated molecular pathways. These key processes enhance photosynthetic stability, osmotic adjustment, and structural remodeling. Additionally, the upregulation of various stress-responsive genes helps RUG maintain a delicate redox balance, countering oxidative stress. The fact that MGT increases proline content under salinity but not drought underscores the importance of osmotic adjustment in drought resilience. This is further evidenced by the healthy xylem vessels in RUG during late stress and recovery stages,

along with sustained photosynthetic performance. We recommend further metabolomic and genomic studies to enhance our understanding of resilience strategies during drought and rewatering phases.

Declaration of competing interest

The authors declare that no conflict of interest exists regarding the completion and publication of this research.

Appendix A. Supplementary data

Supplementary data to this article can be found online at https://doi.org/10.1016/j.plaphy.2025.109618.

Data availability

Data will be made available on request.
PRJNA1045631 (Original data) (NCBI)

References

Ahn, Y.O., Shimizu, B., Sakata, K., Gantulga, D., Zhou, C., Bevan, D.R., Esen, A., 2010. Scopolin-hydrolyzing β-glucosidases in roots of *Arabidopsis*. Plant Cell Physiol. 51, 132–143. https://doi.org/10.1093/pcp/pcp174.

Anil Kumar, S., Hima Kumari, P., Shravan Kumar, G., Mohanalatha, C., Kavi Kishor, P.B., 2015. Osmotin: a plant sentinel and a possible agonist of mammalian adiponectin. Front. Plant Sci. 6, 163. https://doi.org/10.3389/fpls.2015.00163.

Apel, K., Hirt, H., 2004. Reactive oxygen species: metabolism, oxidative stress, and signal transduction. Annu. Rev. Plant Biol. 55, 373–399. https://doi.org/10.1146/annurev.arplant.55.031903.141701.

Bianchi, D., Caramanico, L., Grossi, D., Brancadoro, L., Lorenzis, G., 2020. How do novel M-rootstock (*Vitis* Spp.) genotypes cope with drought? Plants 9, 1385. https://doi.org/10.3390/plants9101385.

Bindea, G., Mlecnik, B., Hackl, H., Charoentong, P., Tosolini, M., Kirilovsky, A., Fridman, W.H., Pagès, F., Trajanoski, Z., Galon, J., 2009. ClueGO: a Cytoscape plug-in to decipher functionally grouped gene ontology and pathway annotation networks. Bioinformatics 25, 1091–1093. https://doi.org/10.1093/bioinformatics/btp101.

Bohnert, H.J., Shen, B.O., 1998. Transformation and compatible solutes. Sci. Hortic. 78, 237–260. https://doi.org/10.1016/S0304-4238(98)00195-2.

Bolger, A.M., Lohse, M., Usadel, B., 2014. Trimmomatic: a flexible trimmer for Illumina sequence data. Bioinformatics 30, 2114–2120. https://doi.org/10.1093/bioinformatics/btu170.

Bradford, M.M., 1976. A rapid and sensitive method for the quantitation of microgram quantities of protein utilizing the principle of protein-dye binding. Anal. Biochem. 72, 248–254. https://doi.org/10.1006/abio.1976.9999.

Brodersen, C.R., McElrone, A.J., 2013. Maintenance of xylem network transport capacity: a review of embolism repair in vascular plants. Front. Plant Sci. 4, 108. https://doi.org/10.3389/fpls.2013.00108.

Cochard, H., Herbette, S., Barigah, T., Badel, E., Ennajeh, M., Vilagrosa, A., 2010. Does sample length influence the shape of xylem embolism vulnerability curves? A test with the Cavitron spinning technique. Plant Cell Environ. 33, 1543–1552. https://doi.org/10.1111/j.1365-3040.2010.02163.x.

Conway, J.R., Lex, A., Gehlenborg, N., 2017. UpSetR: an R package for the visualization of intersecting sets and their properties. Bioinformatics 33, 2938–2940. https://doi.org/10.1093/bioinformatics/btx364, 2017.

Cruz de Carvalho, M.H., 2008. Drought stress and reactive oxygen species: production, scavenging and signaling. Plant Signal. Behav. 3, 156–165. https://doi.org/10.4161/psb.3.3.5536.

Dao, T.T., Linthorst, H.J., Verpoorte, R., 2011. Chalcone synthase and its functions in plant resistance. Phytochem. Rev. 10, 397–412. https://doi.org/10.1007/s11101-011-9211-7.

Das, K., Roychoudhury, A., 2014. Reactive oxygen species (ROS) and response of antioxidants as ROS-scavengers during environmental stress in plants. Front. Environ. Sci. 2, 53. https://doi.org/10.3389/fenvs.2014.00053.

Dietz, K.J., Sauter, A., Wichert, K., Messdaghi, D., Hartung, W., 2000. Extracellular beta-glucosidase activity in barley involved in the hydrolysis of ABA glucose conjugate in leaves. J. Exp. Bot. 51, 937–944. https://doi.org/10.1093/jexbot/51.346.937.

Dobin, A., Davis, C.A., Schlesinger, F., Drenkow, J., Zaleski, C., Jha, S., Batut, P., Chaisson, M., Gingeras, T.R., 2013. STAR: ultrafast universal RNA-seq aligner. Bioinformatics 29, 15–21. https://doi.org/10.1093/bioinformatics/bts635.

Du, W., Yang, J., Li, Q., Jiang, W., Pang, Y., 2024. *Medicago truncatula* β-glucosidase 17 contributes to drought and salt tolerance through antioxidant flavonoid accumulation. Plant Cell Environ. 47, 3076–3089. https://doi.org/10.1111/pce.14928.

Duan, Y., Yang, L., Zhu, H., Zhou, J., Sun, H., Gong, H., 2021. Structure and expression analysis of sucrose phosphate synthase, sucrose synthase, and invertase gene families in *Solanum lycopersicum*. Int. J. Mol. Sci. 22, 4698. https://doi.org/10.3390/ijms22094698.

El Kayal, W., Paliyath, G., Sullivan, J.A., Subramanian, J., 2017. Phospholipase D inhibition by hexanal is associated with calcium signal transduction events in raspberry. Hortic. Res. 4, 17042. https://doi.org/10.1038/hortres.2017.42.

Flexas, J., Ribas-Carbó, M., Bota, J., Galmés, J., Henkle, M., Martínez-Cañellas, S., Medrano, H., 2006. Decreased Rubisco activity during water stress is not induced by decreased relative water content but related to conditions of low stomatal conductance and chloroplast CO_2 concentration. New Phytol. 172, 73–82. https://doi.org/10.1111/j.1469-8137.2006.01794.x.

Gajjar, P., Ismail, A., Islam, T., Darwish, A.G., Moniruzzaman, M., Abuslima, E., Dawood, A.S., El-Saady, A.M., Tsolova, V., El-Kereamy, A., Nick, P., Sherif, S.M., Abazinge, M.D., El-Sharkawy, I., 2023. Physiological comparison of two salt-excluder hybrid grapevine rootstocks under salinity reveals different adaptation qualities. Plants 12, 3247. https://doi.org/10.3390/plants12183247.

Gajjar, P., Ismail, A., Islam, T., Moniruzzaman, M., Darwish, A.G., Dawood, A.S., Mohamed, A.G., Haikal, A.M., El-Saady, A.M., El-Kereamy, A., Sherif, S.M., Abazinge, M.D., Kambiranda, D., El-Sharkawy, I., 2024. Transcriptome profiling of a salt excluder hybrid grapevine rootstock 'Ruggeri' throughout salinity. Plants 13, 837. https://doi.org/10.3390/plants13060837.

Gambetta, G.A., Herrera, J.C., Dayer, S., Feng, Q., Hochberg, U., Castellarin, S.D., 2020. The physiology of drought stress in grapevine: towards an integrative definition of drought tolerance. J. Exp. Bot. 71, 4658–4676. https://doi.org/10.1093/jxb/eraa245.

Ghosh, U.K., Islam, M.N., Siddiqui, M.N., Cao, X., Khan, M.A.R., 2022. Proline, a multifaceted signalling molecule in plant responses to abiotic stress: understanding the physiological mechanisms. Plant Biol. 24, 227–239. https://doi.org/10.1111/plb.13363.

Ginouves, M., Carme, B., Couppie, P., Prevot, G., 2014. Comparison of tetrazolium salt assays for evaluation of drug activity against *Leishmania* spp. J. Clin. Microbiol. 52, 2131–2138. https://doi.org/10.1128/JCM.00201-14.

Haghpanah, M., Hashemipetroudi, S., Arzani, A., Araniti, F., 2024. Drought tolerance in plants: physiological and molecular responses. Plants 13, 2962. https://doi.org/10.3390/plants13212962.

Hasanuzzaman, M., Zhou, M., Shabala, S., 2023. How does stomatal density and residual transpiration contribute to osmotic stress tolerance? Plants 12, 494. https://doi.org/10.3390/plants12030494.

Hosseinifard, M., Stefaniak, S., Ghorbani Javid, M., Soltani, E., Wojtyla, Ł., Garnczarska, M., 2022. Contribution of exogenous proline to abiotic stresses tolerance in plants: a review. Int. J. Mol. Sci. 23, 5186. https://doi.org/10.3390/ijms23095186.

Hsu, P., Dubeaux, G., Takahashi, Y., Schroeder, J.I., 2020. Signaling mechanisms in abscisic acid-mediated stomatal closure. Plant J. 105, 307–321. https://doi.org/10.1111/tpj.15067.

Ingel, B., Reyes, C., Massonnet, M., Boudreau, B., Sun, Y., Sun, Q., McElrone, A.J., Cantu, D., Roper, M.C., 2020. *Xylella fastidiosa* causes transcriptional shifts that precede tylose formation and starch depletion in xylem. Mol. Plant Pathol. 22, 175–188. https://doi.org/10.1111/mpp.13016.

Islam, M.T., Lee, B.R., Park, S.H., La, V.H., Bae, D.W., Kim, T.H., 2017. Cultivar variation in hormonal balance is a significant determinant of disease susceptibility to *Xanthomonas campestris* pv. campestris in *Brassica napus*. Front. Plant Sci. 8, 2121. https://doi.org/10.3389/fpls.2017.02121.

Ismail, A., Takeda, S., Nick, P., 2014. Life and death under salt stress: same players, different timing? J. Exp. Bot. 65, 2963–2979. https://doi.org/10.1093/jxb/eru159.

Ismail, A., El-Sharkawy, I., Sherif, S., 2020. Salt stress signals on demand: cellular events in the right context. Int. J. Mol. Sci. 21, 3918. https://doi.org/10.3390/ijms21113918.

Ismail, A., Gajjar, P., Park, M., Mahboob, A., Tsolova, V., Jayasankar, S., Darwish, A.G., El-Sharkawy, I., 2022. A recessive mutation in muscadine grapes causes berry color-loss without influencing anthocyanin pathway. Commun. Biol. 5, 1012. https://doi.org/10.1038/s42003-022-04001-8.

Khandelwal, A., Elvitigala, T., Ghosh, B., Quatrano, R.S., 2008. *Arabidopsis* transcriptome reveals control circuits regulating redox homeostasis and the role of an AP2 transcription factor1. Plant Physiol. 148, 2050–2058. https://doi.org/10.1104/pp.108.128488.

Kim, J.S., Kidokoro, S., Yamaguchi-Shinozaki, K., Shinozaki, K., 2024. Regulatory networks in plant responses to drought and cold stress. Plant Physiol. 195, 170–189. https://doi.org/10.1093/plphys/kiae105.

Kolberg, L., Raudvere, U., Kuzmin, I., Adler, P., Vilo, J., Peterson, H., 2023. g: Profiler—interoperable web service for functional enrichment analysis and gene identifier mapping (2023 update). Nucleic Acids Res. 51, W207–W212. https://doi.org/10.1093/nar/gkad347.

Lafarguette, F., Leple, J.C., Dejardin, A., Laurans, F., Costa, G., Lesage-Descauses, M.C., Pilate, G., 2004. Poplar genes encoding fasciclin-like arabinogalactan proteins are highly expressed in tension wood. New Phytol. 164, 107–121. https://doi.org/10.1111/j.1469-8137.2004.01175.x.

Lawlor, D.W., Tezara, W., 2009. Causes of decreased photosynthetic rate and metabolic capacity in water-deficient leaf cells: a critical evaluation of mechanisms and integration of processes. Ann. Bot. 103, 561–579. https://doi.org/10.1093/aob/mcn244.

Lee, K.H., Piao, H.L., Kim, H.Y., Choi, S.M., Jiang, F., Hartung, W., Hwang, I., Kwak, J.M., Lee, I.J., Hwang, I., 2006. Activation of glucosidase via stress-induced polymerization rapidly increases active pools of abscisic acid. Cell 126, 1109–1120. https://doi.org/10.1016/j.cell.2006.07.034.

Lee, B.R., Muneer, S., Park, S.H., Zhang, Q., Kim, T.H., 2013. Ammonium-induced proline and sucrose accumulation, and their significance in antioxidative activity and osmotic adjustment. Acta Physiol. Plant. 35, 2655–2664. https://doi.org/10.1007/s11738-013-1297-7.

Love, M.I., Huber, W., Anders, S., 2014. Moderated estimation of fold change and dispersion for RNA-seq data with DESeq2. Genome Biol. 15, 550. https://doi.org/10.1186/s13059-014-0550-8.

Ma, Y., Shafee, T., Mudiyanselage, A.M., Ratcliffe, J., MacMillan, C.P., Mansfield, S.D., Bacic, A., Johnson, K.L., 2023. Distinct functions of *FASCILIN-LIKE ARABINOGALACTAN PROTEINS* relate to domain structure. Plant Physiol. 192, 119–132. https://doi.org/10.1093/plphys/kiad284.

MacMillan, C.P., Mansfield, S.D., Stachurski, Z.H., Evans, R., Southerton, S.G., 2010. Fasciclin-like arabinogalactan proteins: specialization for stem biomechanics and cell wall architecture in *Arabidopsis* and *Eucalyptus*. Plant J. 62, 689–703. https://doi.org/10.1111/j.1365-313X.2010.04181.x.

Madumane, K., Sewelo, L.T., Nkane, M.N., Batlang, U., Malambane, G., 2024. Morphological, physiological, and molecular stomatal responses in local watermelon landraces as drought tolerance mechanisms. Horticulturae 10, 123. https://doi.org/10.3390/horticulturae10020123.

Matsuo, M., Oelmüller, R., 2015. *REDOX RESPONSIVE TRANSCRIPTION FACTOR1* is involved in age-dependent and systemic stress signaling. Plant Signal. Behav. 10, e1051279. https://doi.org/10.1080/15592324.

Matsuo, M., Johnson, J.M., Hieno, A., Tokizawa, M., Nomoto, M., Tada, Y., Godfrey, R., Obokata, J., Sherameti, I., Yamamoto, Y.Y., Böhmer, F.D., Oelmüller, R., 2015. High *REDOX RESPONSIVE TRANSCRIPTION FACTOR1* levels result in accumulation of reactive oxygen species in *Arabidopsis thaliana* shoots and roots. Mol. Plant 8, 1253–1273. https://doi.org/10.1016/j.molp.2015.03.011.

Miller, G., Suzuki, N., Ciftci-Yilmaz, S., Mittler, R., 2010. Reactive oxygen species homeostasis and signalling during drought and salinity stresses. Plant Cell Environ. 33, 453–467. https://doi.org/10.1111/j.1365-3040.2009.02041.x.

Minocha, R., Martinez, G., Lyons, B., Long, S., 2009. Development of a standardized methodology for quantifying total chlorophyll and carotenoids from foliage of hardwood and conifer tree species. Can. J. For. Res. 39, 849–861. https://doi.org/10.1139/x09-015.

Mishra, G., Zhang, W., Deng, F., Zhao, J., Wang, X., 2006. A bifurcating pathway directs abscisic acid effects on stomatal closure and opening in *Arabidopsis*. Science 312, 264–266. https://doi.org/10.1126/science.1123769.

Mittler, R., Zandalinas, S.I., Fichman, Y., Van Breusegem, F., 2022. Reactive oxygen species signalling in plant stress responses. Nat. Rev. Mol. Cell Biol. 23, 663–679. https://doi.org/10.1038/s41580-022-00499-2.

Moreno, J., García-Murria, M.J., Marín-Navarro, J., 2008. Redox modulation of Rubisco conformation and activity through its cysteine residues. J. Exp. Bot. 59, 1605–1614. https://doi.org/10.1093/jxb/erm310.

Nagahatenna, D.S., Langridge, P., Whitford, R., 2015. Tetrapyrrole-based drought stress signalling. Plant Biotechnol. J. 13, 447–459. https://doi.org/10.1111/pbi.12356.

Nardini, A., Lo Gullo, M.A., Salleo, S., 2011. Refilling embolized xylem conduits: is it a matter of phloem unloading? Plant Sci. 180, 604–611. https://doi.org/10.1016/j.plantsci.2010.12.011.

Nour, M.M., Aljabi, H.R., AL-Huqail, A.A., Horneburg, B., Mohammed, A.E., Alotaibi, M. O., 2024. Drought responses and adaptation in plants differing in life-form. Front. Ecol. Evol. 12, 1452427. https://doi.org/10.3389/fevo.2024.1452427.

Park, E.J., Kim, T.H., 2021. *Arabidopsis OSMOTIN 34* functions in the ABA signaling pathway and is regulated by proteolysis. Int. J. Mol. Sci. 22, 7915. https://doi.org/10.3390/ijms22157915.

Patro, R., Duggal, G., Love, M.I., Irizarry, R.A., Kingsford, C., 2017. Salmon: fast and bias-aware quantification of transcript expression using dual-phase inference. Nat. Methods 14, 417–419. https://doi.org/10.1038/nmeth.4197.

Peiró, R., Jiménez, C., Perpiñà, G., Soler, J.X., Gisbert, C., 2020. Evaluation of the genetic diversity and root architecture under osmotic stress of common grapevine rootstocks and clones. Sci. Hortic. 266, 109283. https://doi.org/10.1016/j.scienta.2020.109283.

Phung, T.H., Jung, H.I., Park, J.H., Kim, J.G., Back, K., Jung, S., 2011. Porphyrin biosynthesis control under water stress: sustained porphyrin status correlates with drought tolerance in transgenic rice. Plant Physiol. 157, 1746–1764. https://doi.org/10.1104/pp.111.188276.

Pinheiro, C., Chaves, M.M., 2011. Photosynthesis and drought: can we make metabolic connections from available data? J. Exp. Bot. 62, 869–882. https://doi.org/10.1093/jxb/erq340.

Pouzoulet, J., Scudiero, E., Schiavon, M., Santiago, L.S., Rolshausen, P.E., 2019. Modeling of xylem vessel occlusion in grapevine. Tree Physiol. 39, 1438–1445. https://doi.org/10.1093/treephys/tpz036.

Raghothama, K.G., Maggio, A., Narasimhan, M.L., Kononowicz, A.K., Wang, G.L., D'Urzo, M.P., Hasegawa, P.M., Bressan, R.A., 1997. Tissue-specific activation of the osmotin gene by ABA, C_2H_4, and NaCl involves the same promoter region. Plant Mol. Biol. 34, 393–402. https://doi.org/10.1023/A:1005812217945.

Rajput, V.D., Harish, Singh, R.K., Verma, K.K., Sharma, L., Quiroz-Figueroa, F.R., Meena, M., Gour, V.S., Minkina, T., Sushkova, S., Mandzhieva, S., 2021. Recent developments in enzymatic antioxidant defence mechanism in plants with special reference to abiotic stress. Biology 10, 267. https://doi.org/10.3390/biology10040267.

Rehman, A.U., Bashir, F., Ayaydin, F., Kóta, Z., Páli, T., Vass, I., 2021. Proline is a quencher of singlet oxygen and superoxide both in *in vitro* systems and isolated thylakoids. Physiol. Plantarum 172, 7–18. https://doi.org/10.1111/ppl.13265.

Shinozaki, K., Uemura, M., Bailey-Serres, J., Bray, E.A., Weretilnyk, E., 2015. Plant environment and agriculture: responses to abiotic stress. In: Buchanan, B.B., Gruissem, W., Jones, R.L. (Eds.), Biochemistry & Molecular Biology of Plants, second ed. John Wiley & Sons, Ltd., Hoboken, NJ, USA, pp. 1051–1100.

Smeekens, S., 2000. Sugar-induced signal transduction in plants. Annu. Rev. Plant Physiol. Plant Mol. Biol. 51, 49–81. https://doi.org/10.1146/annurev.arplant.51.1.49.

Srivastava, A., Malik, L., Sarkar, H., Zakeri, M., Almodaresi, F., Soneson, C., Love, M.I., Kingsford, C., Patro, R., 2020. Alignment and mapping methodology influence transcript abundance estimation. Genome Biol. 21, 239. https://doi.org/10.1186/s13059-020-02151-8.

Sun, Q., Sun, Y., Walker, M.A., Labavitch, J.M., 2013. Vascular occlusions in grapevines with Pierce's disease make disease symptom development worse. Plant Physiol. 161, 1529–1541. https://doi.org/10.1104/pp.112.208157.

Sun, T., Li, M., Shao, Y., Yu, L., Ma, F., 2017. Comprehensive genomic identification and expression analysis of the phosphate transporter (PHT) gene family in apple. Front. Plant Sci. 8, 426. https://doi.org/10.3389/fpls.2017.00426.

Takahashi, F., Kuromori, T., Urano, K., Yamaguchi-Shinozaki, K., Shinozaki, K., 2020. Drought stress responses and resistance in plants: from cellular responses to long-distance intercellular communication. Front. Plant Sci. 11, 556972. https://doi.org/10.3389/fpls.2020.556972.

Tanaka, R., Kobayashi, K., Masuda, T., 2011. Tetrapyrrole metabolism in *Arabidopsis thaliana*. Arabidopsis Book 9, e0145. https://doi.org/10.1199/tab.0145.

Turner, N.C., 2018. Turgor maintenance by osmotic adjustment: 40 years of progress. J. Exe. Bot. 69, 3223–3233. https://doi.org/10.1093/jxb/ery181.

Wang, C., Chen, S., Dong, Y., Ren, R., Chen, D., Chen, X., 2020. Chloroplastic *Os3BGlu6* contributes significantly to cellular ABA pools and impacts drought tolerance and photosynthesis in rice. New Phytol. 226, 1042–1054. https://doi.org/10.1111/nph.16416.

Wang, Z., Yang, Y., Yadav, V., Zhao, W., He, Y., Zhang, X., Wei, C., 2022. Drought-induced proline is mainly synthesized in leaves and transported to roots in watermelon under water deficit. Hortic. Plant J. 8, 615–626. https://doi.org/10.1016/j.hpj.2022.06.009.

Warzecha, H., Gerasimenko, I., Kutchan, T.M., Stockigt, J., 2000. Molecular cloning and functional bacterial expression of a plant glucosidase specifically involved in alkaloid biosynthesis. Phytochemistry 54, 657–666. https://doi.org/10.1016/s0031-9422(00)00175-8.

Waszczak, C., Carmody, M., Kangasjärvi, J., 2018. Reactive oxygen species in plant signaling. Annu. Rev. Plant Biol. 69, 209–236. https://doi.org/10.1146/annurev-arplant-042817-040322.

Yang, Z., Li, J.L., Liu, L.N., Xie, Q., Sui, N., 2020. Photosynthetic regulation under salt stress and salt-tolerance mechanism of sweet sorghum. Front. Plant Sci. 10, 1722. https://doi.org/10.3389/fpls.2019.01722.

Yao, K., Yao, Y., Ding, Z., Pan, X., Zheng, Y., Huang, Y., Zhang, Z., Li, A., Wang, C., Li, C., Liao, W., 2023. Characterization of the FLA gene family in tomato (*Solanum lycopersicum* L.) and the expression analysis of *SlFLAs* in response to hormone and abiotic stresses. Int. J. Mol. Sci. 24, 16063. https://doi.org/10.3390/ijms242216063.

Yuan, G., Qian, Y., Ren, Y., Guan, Y., Wu, X., Ge, C., Ding, H., 2021. The role of plant-specific VQ motif-containing proteins: an ever-thickening plot. Plant Physiol. Biochem. 159, 12–16. https://doi.org/10.1016/j.plaphy.2020.12.005.

Zhang, Z., Xin, W., Wang, S., Zhang, X., Dai, H., Sun, R., Frazier, T., Zhang, B., Wang, Q., 2015. Xylem sap in cotton contains proteins that contribute to environmental stress response and cell wall development. Funct. Integr. Genom. 15, 17–26. https://doi.org/10.1007/s10142-014-0395-y.

Zhang, L., Zheng, Y., Xiong, X., Li, H., Zhang, X., Song, Y., Zhang, X., Min, D., 2023. The wheat VQ motif-containing protein *TaVQ4-D* positively regulates drought tolerance in transgenic plants. J. Exp. Bot. 74, 5591–5605. https://doi.org/10.1093/jxb/erad280.

Zhao, J.Y., Lu, Z.W., Sun, Y., Fang, Z.W., Chen, J., Zhou, Y.B., Chen, M., Ma, Y.Z., Xu, Z. S., Min, D.H., 2020. The ankyrin-repeat gene *GmANK114* confers drought and salt tolerance in *Arabidopsis* and soybean. Front. Plant Sci. 11, 584167. https://doi.org/10.3389/fpls.2020.584167.